Iris Marijke Elisa Janssen

Model improvement for a dynamic pH carbonate system under different salinities applicable for soft sensors in microalgae photobioreactors

MSc Thesis | Department of Bioprocess Engineering | Wageningen University & Research

WAGENINGEN
UNIVERSITY & RESEARCH

Model improvement for a dynamic pH carbonate system under different salinities applicable to soft sensors in microalgae photobioreactors

By
I. M. E. Janssen
1021072

MSc Thesis
Published on the 21st of July 2023

Under the supervision of
Dipl.-Ing. Henrik Geltner

Submitted to the examiner
Dr.ir. Marcel Janssen

At the Department of
Bioprocess Engineering, Wageningen University & Research

In the partial fulfillment of the requirements for the degree
MSc Biotechnology

WAGENINGEN
UNIVERSITY & RESEARCH

Abstract

Soft sensors offer valuable applications in process technology, including pH control in bioreactors. Particularly, in the microalgal cultivation sector where the carbonate system plays a crucial role in influencing the pH through the injection CO_2. Here, seawater is often utilized as medium hence requiring the characterization of the dynamic carbonate system at higher salinities. In this report, a MATLAB model is described to predict the pH within a lab-scale photobioreactor based on changes in the carbonate system under different salinities. The model considers the measured off-gas CO_2 concentrations and electrical conductivity measurements as input. It provides estimations for the concentrations of the species present in the carbonate system and calculates the pH over time. The model's predictions align with the changing pH patters observed during the CO_2 variations over time. However, there are slight discrepancies between the predicted pH and measured pH, especially in solutions with higher ionic strengths. To improve accuracy, more precise calibration of the model is needed to determine the cation fit factor, which accounts for the surplus of cations present in the solution.

Nomenclature

Symbols

γ_i	Activity coefficient of component i	$[\text{-}]$
a_i	Activity of component i	$[mol\ L^{-1}]$
c_i	Concentration of component i	$[mol\ L^{-1}]$
c_i^*	Saturation concentration of component i	$[mol\ L^{-1}]$
D_L	Dilution rate of the photobioreactor	$[s^{-1}]$
F_{CO_2}	Mass transfer rate of CO_2	$[mol\ L^{-1}\ s^{-1}]$
F_G	Gas flow rate	$[L\ s^{-1}]$
H_{CO2}	Henry coefficient for CO_2	$[mol\ L^{-1}\ bar^{-1}]$
I	Ionic strength	$[mol\ L^{-1}]$
K_i	Equilibrium constant of reaction i	$[\text{-}]$
$k_l a$	Mass transfer coefficient	$[s^{-1}]$
n_i	Mole mass	$[mol]$
P	Partial pressure	$[Pa]$
T	Temperature	$[K]$
t	Time	$[s]$
x_i	Mole fraction of component i	$[\text{-}]$
z_i	Charge of ion i	$[\text{-}]$

Abbreviations

DIC	Dissolved Inorganic Carbon
ODE	Ordinary Differential Equation
ASW	Artificial Seawater
$RMSE$	Root Mean Square Error

Table of Contents

1. Introduction

Soft sensors, also known as virtual sensors, can be devoted to the estimation of variables in plants controlling the process (Tham et al., 1991). The sensors offer multiple advantages such as the realization of a less expensive alternative for hardware sensor devices and the input for more comprehensive monitoring networks. Moreover, soft sensors allow real-time data and parameter estimation to which no hardware sensor is applicable, hence improving control strategy performances (Fortuna, 2007; Jiang et al., 2021; Tham et al., 1991). Understanding the mathematical model of the process is critical to construct the soft sensor.

An application for soft sensors can be found in process technology, such as in the microalgal cultivation sector. Cultivation of microalgae caught the attention of the scientific community since the valorization of the produced algal biomass assures nutrient recovery and CO_2 fixation (Guldhe et al., 2017). Parameters of a microalgae photobioreactor such as light, temperature, and pH can be modeled dynamically within soft sensors lowering costs and increasing the reliability of the cultivation process (González-Camejo et al., 2020). González-Camejo et al. (2020) established the possibility of a soft sensor application for the online monitoring of photosynthetic activity based on pH data.

In microalgal photobioreactors, microalgae cultures are influenced by pH changes both directly, as each species has an optimal range of pH for growth, and indirectly, as nutrient availability is affected (Suh & Lee, 2003). Inversely, the pH in the photobioreactor is influenced by nutrient consumption. When the pH would be accurately modeled and controlled, the ability to estimate these nutrient uptake rates would arise. Fundamentally, the carbonate system, as described above, will influence the pH. To provide substrate for autotrophic microalgal cultivation, CO_2 gas is injected and subsequently absorbed (Ifrim et al., 2014). The supply of CO_2 assures a decrease in pH, as CO_2 is converted to carbonic acid (H_2CO_3) and bicarbonate (HCO_3^-), which can dissociate to produce hydrogen ions (H^+). This way, CO_2 gas injection gives a possibility to control the pH in the microalgal systems, as the pH is dependent on the hydration, dehydration, and protonation of CO_2 (Berenguel et al., 2004).

Moreover, pH correlates to the activity of protons that subsequently depends on the salinity of the medium (Buck et al., 2002). Activity coefficients play a significant role since they lower in a more saline solution, as described by the Davies approximation (Stumm, 1996). These interdependencies of equations describing species concentrations within the carbonate system, activity coefficients, and pH, assure the need for a mathematical model. Careful modeling of both the activity coefficient and concentration of protons is crucial in the design of this dynamic carbonate model defining pH behavior.

In this report, a model is described to predict the pH within a bioreactor based on changes in the carbonate system under different salinities. First, more in-depth theoretical background on the dynamic carbonate system and activity coefficients is given. Subsequently, materials and methods are reported for model development in MATLAB as well as the calibration and validation of the model on a lab-scale flat panel photobioreactor. Next, the results of these experiments are shown and discussed. Lastly, further research recommendations are given based on the results and conclusions.

2. Theoretical background

Developing a soft sensor for the pH control of bioprocesses requires knowledge of both soft sensor development and the factors that influence pH. To describe the characteristics of the model predicting pH, the dynamic carbonate system is explained, and equations describing component concentrations within the carbonate system will be established. Moreover, the influence of medium salinities on these concentration dynamics will be specified.

Chapter 2 starts with a section dedicated to soft sensor development and highlights challenges encountered in the field. The subsequent sections focus on the carbonate system, which plays a significant role in pH dynamics. The conversion term within the predictive model, also known as the carbonate kinetics, will by described to elaborate on the processes occurring. Additionally, the transport dynamics (i.e. gas-liquid transport of CO_2) will be examined. Furthermore, parameters influencing the activity of protons in more saline solutions, particularly the activity coefficients, will be discussed.

2.1 Soft sensor development

Soft sensors applied in the process industry can function as online predictions of process variables, process monitoring or controlling, and process fault detection (Kadlec et al., 2009). The utilization of soft sensors offers several advantages, as mentioned previously. One key advantage is the ability to estimate data in real-time, providing timely and up-to-date information for decision-making and control purposes. Soft sensors also prove helpful in situations where no hardware device or physical sensor is applicable or available. They enable the estimation of critical variables or parameters that cannot be directly measured, thereby expanding the scope of monitoring and control capabilities in various applications (Fortuna, 2007).

To develop a soft sensor, characterization of the process dynamics within the bioreactor is required. Roughly this characterization consists of two types of terms, one defining conversion reactions, and the other transport dynamics. Furthermore, when developing a bioprocess control model distinctions can be made between state variables and process parameters (Dochain, 2013). The dynamics of state variables, primarily component concentrations, are described by the differential equations and process parameters. Examples of these process parameters are reaction constants, specific growth rates, or transfer parameters.

The main difficulty during soft sensor development can be found in obtaining accurate process data for model construction. Various obstacles, such as missing values, measurement noise, data drifting, data outliers, and varying sampling rates can hinder the processing of data used in soft sensor development. Addressing these issues requires careful manual work when collecting the data during a process. Efforts must be made to identify and rectify missing data and outliers, mitigate measurement noise, handle data drifting, and ensure consistent sampling rates (Kadlec et al., 2009).

For fault detection during the development of the soft sensor, the parity space method is commonly used, shown in Figure 1. In principle, this method establishes the consistency between the measurements taken and the output given by the mathematical model (Odendaal & Jones, 2014). Naturally, the goal of the model development is to diminish the residual term shown in Figure 1.
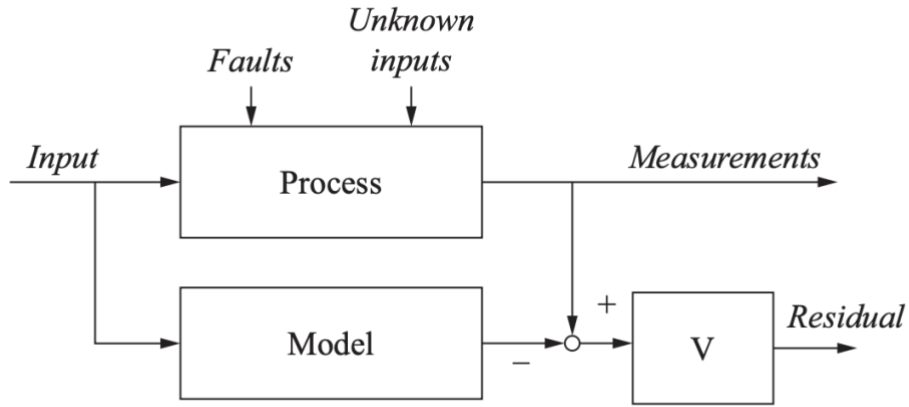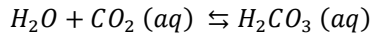
Figure 1. An input-output format of a parity space approach (Dochain, 2013).

2.2 The carbonate system

In a bioreactor system where carbon dioxide (CO_2) is consumed, this process plays a significant role in influencing the medium pH in the reactor (Eriksen et al., 2007). The supply of CO_2 gas into such a reactor ensures gas-liquid transfer, allowing the transfer of the component into the aqueous phase. Subsequently, CO_2 dissociates into carbonic acid (H_2CO_3), bicarbonate (HCO_3^-), and carbonate (CO_3^{2-}) corresponding to Reactions 1, 2, and 3. The formation of protons in these reactions impacts the water equilibrium shown in Reaction 4.
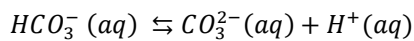
Reaction 1

$$H_2O + CO_2\ (aq) \leftrightharpoons H_2CO_3\ (aq)$$

Reaction 2

$$H_2CO_3\ (aq) \leftrightharpoons HCO_3^-\ (aq) + H^+(aq)$$

Reaction 3

$$HCO_3^-\ (aq) \leftrightharpoons CO_3^{2-}(aq) + H^+(aq)$$

Reaction 4

$$H_2O \leftrightharpoons H^+(aq) + OH^-(aq)$$
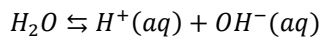
It is important to note that carbonic acid shows to react very rapidly into bicarbonate reasoning the common assumption to neglect this first hydration reaction (Stumm, 1996).

This interplay of reactions explains the influence of CO_2 on the pH of the medium. When the concentrations of species shift towards carbonate formation, the pH of the medium decreases. Conversely, an increase in pH indicates a shift towards aqueous carbon dioxide. Figure 2 illustrates this relationship in an open carbonate system (Zeebe & Wolf-Gladrow, 2001). In an open carbonate system, the aqueous solution is capable of reaching equilibrium with atmospheric CO_2. Consequently, as pH decreases, the total amount of dissolved inorganic carbon (DIC) increases. Adversely, in a closed system, where the

amount of DIC remains constant when pH increases. Here, the equilibria between the carbonate species are restricted by the absence of atmospheric CO_2 exchange (Stumm, 1996). In more detail, the summation of dissolved components present in the carbonate system (i.e. CO_2, HCO_3^- and CO_3^{2-}) is termed Dissolved Inorganic Carbon (DIC) (Zeebe & Wolf-Gladrow, 2001).

$$DIC = [CO_2] + [HCO_3^-] + [CO_3^{2-}]$$ 　　　　　　　　　　Equation 1
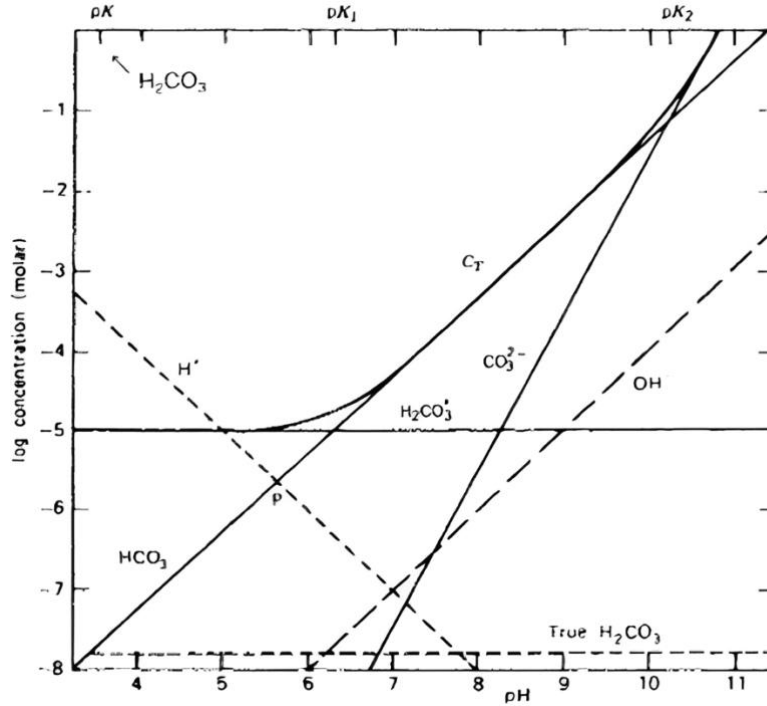
Figure 2. The open carbonate system at atmospheric pressure and 25 degrees Celsius (Stumm, 1996).

Complementary to Reaction 2, 3, and 4, stoichiometric equilibrium constants are given by Equation 2, 3, and 4, respectively (Culberson & Pytkowicz, 1973; Millero et al., 2006).

$$K_1^* = \frac{[H^+][HCO_3^-]}{[CO_2]}$$ 　　　　　　　　Equation 2

$$K_2^* = \frac{[H^+][CO_3^{2-}]}{[HCO_3^-]}$$ 　　　　　　　　Equation 3

$$K_w^* = [H^+][OH^-]$$ 　　　　　　　　Equation 4

Equations 1, 2, and 3 are applicable to an (almost) pure solution where components behave ideally following that their activity coefficient approaches 1. However, in more saline solutions (i.e., non-ideal) the activity of components needs to be considered, as their activity coefficients are lower than 1 due to the increased amount of dissolved ions. The activity of component i is described by Equation 5 (Boom et al., 2021).

$$a_i = x_i \gamma_i$$ 　　　　　　　　Equation 5

Where, x_i is the mole fraction or concentration, and γ_i is the activity coefficient of component i. It is important to note that when using the mole fraction, the activity of the component will be dimensionless. However, when using concentration, the unit of the activity will be the same as the unit of the concentration used.

Consequently, theoretically, the stoichiometric equilibrium constants in solutions of higher salinities are related to the species' activities, following Equations 6, 7, and 8 (Culberson & Pytkowicz, 1973; Millero et al., 2006).

$$K_1 = \frac{\gamma_H \gamma_{HCO_3}}{a_{H_2O}\, \gamma_{CO_2}} K_1^*$$
Equation 6

$$K_2 = \frac{\gamma_H \gamma_{CO_3}}{\gamma_{HCO_3}} K_2^*$$
Equation 7

$$K_w = \frac{\gamma_H \gamma_{OH}}{a_{H_2O}} K_w^*$$
Equation 8

Substitution of the respective stoichiometric equilibrium constants in Equation 6, 7, and 8 establishes the equations for the equilibrium constants under saline conditions given by Equation 9, 10, and 11.

$$K_1 = \frac{\gamma_H \gamma_{HCO_3}}{a_{H_2O}\, \gamma_{CO_2}} \frac{[H^+][HCO_3^-]}{[CO_2]}$$
Equation 9

$$K_2 = \frac{\gamma_H \gamma_{CO_3}}{\gamma_{HCO_3}} \frac{[H^+][CO_3^{2-}]}{[HCO_3^-]}$$
Equation 10

$$K_w = \frac{\gamma_H \gamma_{OH}}{a_{H_2O}} [H^+][OH^-]$$
Equation 11

As the amount of dissolved ions increases in more saline solutions, the activity of water (a_{H_2O}) decreases, as described in Equation 12 (Fernández, 2011). Nevertheless, the number of water molecules typically greatly exceeds the number of other ions present. As a result, the term n_2 becomes negligible and a_{H_2O} approaches a value of 1. Hence, commonly, the activity of water is nearly equal to its concentration and behaves as an ideal component in the solution.

$$a_{H_2O} = \frac{n_1}{n_1 + n_2}$$
Equation 12

Where, n_1 and n_2 are moles of water and solute, respectively.

The equilibrium constants in Equations 9 and 10 are dependent on both salinity and temperature. In more saline solutions, the activity coefficients of the components play a significant role. These activity coefficients have an impact on the value of the equilibrium constants, as they are based on component activity. Additionally, temperature variations can also influence the equilibria reactions. Higher temperatures generally enhance the solubility of salts, allowing for a greater number of ions in the solution. This temperature dependence affects the equilibrium constants and the overall behavior of the system.

Millero et al. (2006) established the relationship between the pK_i, S and T, as described in Equation 13 with its constant parameters in Table 1.

$$pK_i - pK_i^0 = A_i + \frac{B_i}{T} + C_i \ln(T)$$ Equation 13

Pure water references for pK_2^0 and pK_2^0 are described earlier (Harned & Davis, 1943; Harned & Scholes, 1941). The relation between pK_i and K_i is defined by Equation 14.

$$K_i = 10^{-pK_i}$$ Equation 14

Table 1. Parameters for the determination of the dissociation constants pK_1 and pK_2 as a function of ionic strength and temperature (Millero et al., 2006).

	pK_1	pK_2
pK_i^0	$-126.34048 + \dfrac{6320.813}{T} + 19.568224 \ln(T)$	$-90.18333 + \dfrac{5143.692}{T} + 14.613358 \ln(T)$
A_i	$93.9053 I^{0.5} + 1.6549 I - 0.130 I^2$	$147.2748 I^{0.5} + 6.0876 I - 0.869 I^2$
B_i	$-3706.9 I^{0.5} - 303.7 I$	$-5400.9 I^{0.5} - 968.4 I$
C_i	$-14.4858 I^{0.5}$	$-23.2804 I^{0.5}$

2.3 Activity coefficient

To establish the activity of the components in the solution, single-ion activity coefficients (γ_i) need to be determined. The most important parameter affecting γ_i is the ionic strength (I) of the solution, described by Equation 15.

$$I = \frac{1}{2} \sum c_i z_i^2$$ Equation 15

In this Equation, c_i is the concentration of the species and z_i is the charge of component i.

Equation 15 must consider all charged components present in the reactor to accurately determine the ionic strength of the solution. For dilute solutions with an ionic strength not exceeding 0.1M, activity coefficients are described by the Debye-Hückel equation (Pankow, 2019; Ritsema, 1993) in Equation 16.

$$-\log \gamma_i = A z_i^2 \frac{I^{\frac{1}{2}}}{1 + B\, d\, I^{\frac{1}{2}}}$$ Equation 16

The terms A and B are temperature-dependent constants, z_i is the charge of component i, I is the ionic strength of the solution and, d is the diameter of the ion.

When cultivation media or other solutions carry an ionic strength higher than 0.1M, the Debye-Hückel equation is not applicable. The single-ion activity coefficients in a more concentrated solution differ since ions get in closer proximity influencing ion-pair formation and complexation (Ritsema, 1993). As a result, activity coefficients are lower in more saline solutions. For systems with an ionic strength not exceeding 0.5M, the Davies equation is commonly employed, represented in Equation 17 (Pankow, 2019; Ritsema, 1993).

$$-\log \gamma_i = 0.51 z_i^2 \frac{I^{\frac{1}{2}}}{1 + I^{\frac{1}{2}}} - 0.3 I$$ Equation 17

This logarithmic function describes the ion activity coefficient based on its valence and the ionic strength of the solution. A significant difference in the ion activity of species in solution is found in the distinction between univalent and divalent ions. Lower valance ions have a higher activity coefficient than high valance ions for any ionic strength, as illustrated in Figure 3.
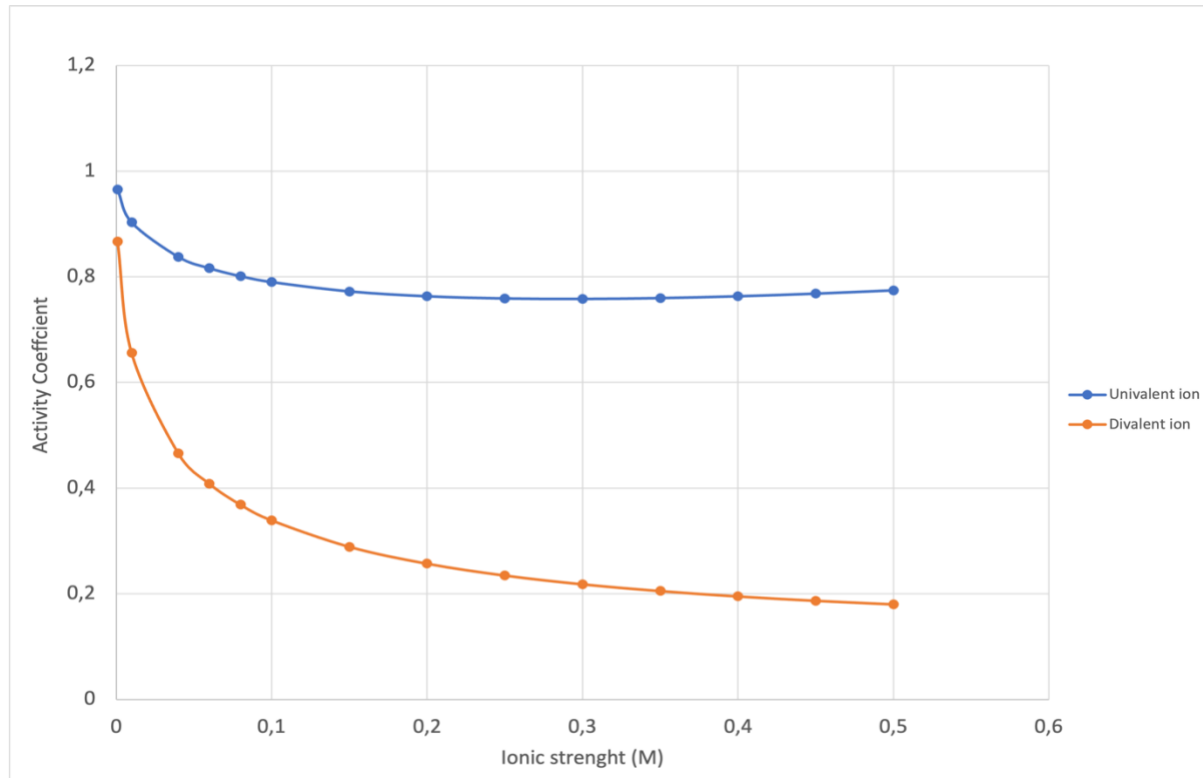

Figure 3. Activity coefficient based on the Davies Equation, valid for solutions with an ionic strength not exceeding 0.5M.

In seawater, where the ionic strength exceeds 0.5M, other relationships are established in order to understand the correlation between the ionic strength and the activity coefficient. Previous studies have derived empirical equations to predict the activity coefficients in these more concentrated solutions (Plummer & Sundquist, 1982; Pytkowicz, 1975; Ulfsbo et al., 2015). These models account for ion-paring and primarily describe mean activity coefficients for salts considering their radii. The ionization behavior of hydroxide ions and protons is described by Culberson & Pytkowicz (1973) and presented in Figure 4. Additionally, the activity coefficients of bicarbonate and carbonate ions as a function of the ionic strength are illustrated in Figure 4 (Pytkowicz, 1975). The empirical relationships between the activity coefficients and higher ionic strength in more saline solutions are presented in Table 2.

Table 2. Empirical relationships between the activity coefficient and ionic strength of the species within the carbonate system in solutions with an ionic strength higher than 0.5M.

Species	Equation describing the relation between its activity coefficient and the ionic strength of the solution		Reference
HCO_3^-	$\gamma_{HCO_3^-} = -0.276\,I + 0.684$	$(R^2 = 1)$	(Pytkowicz, 1975)
CO_3^{2-}	$\gamma_{CO_3^{2-}} = -0.069\,I + 0.078$	$(R^2 = 0.99)$	(Pytkowicz, 1975)
OH^-	$\gamma_{OH^-} = -0.266\,I + 0.407$	$(R^2 = 0.98)$	(Culberson & Pytkowicz, 1973)
H^+	$\gamma_{H^+} = 0.073\,I + 0.664$	$(R^2 = 0.90)$	(Culberson & Pytkowicz, 1973)
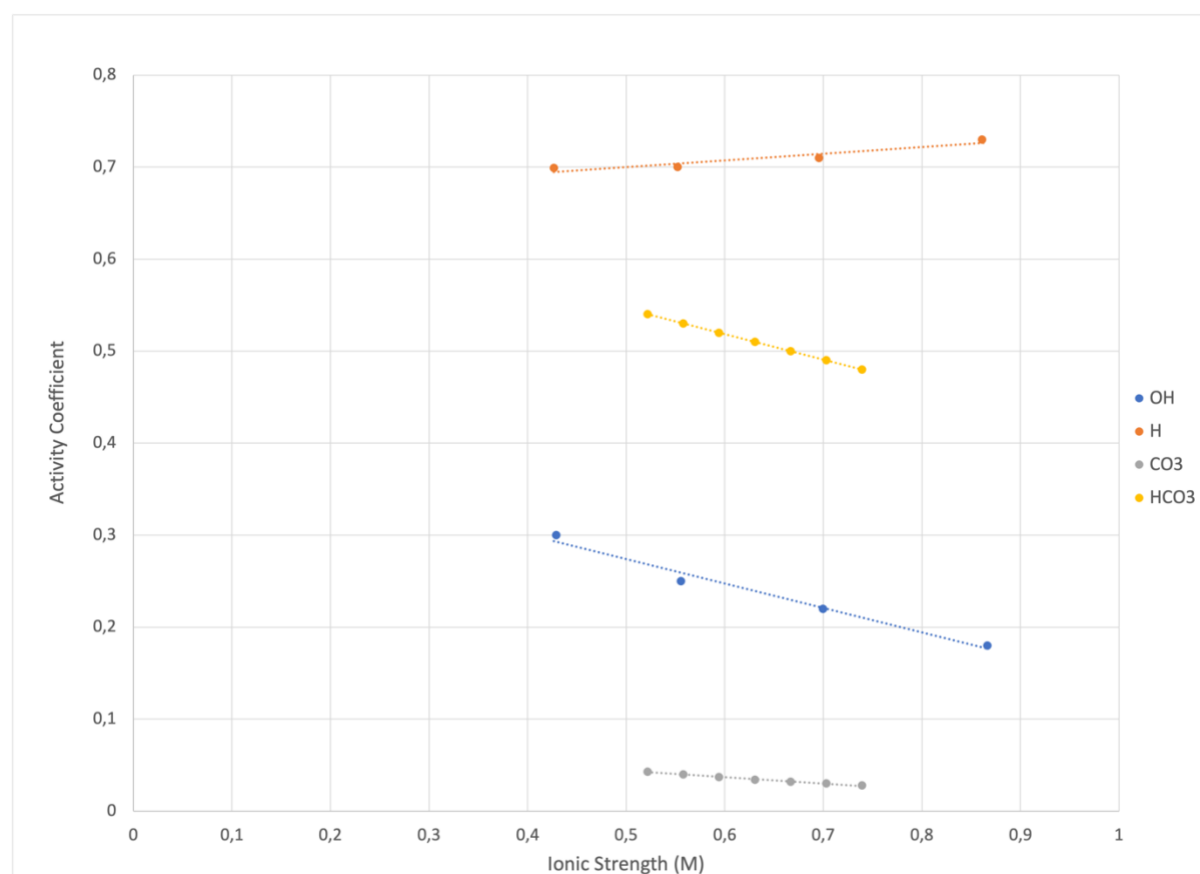
Figure 4. Activity coefficients of H^+, OH^-, HCO_3^-, and CO_3^{2-} in more saline solutions.

It is important to note that ionic strength is not directly measured, as it involves quantifying the total concentration of all ions present in a solution. Therefore, an indirect approach is commonly employed, based on its correlation with electrical conductivity. Here, the underlying principle is that the presence of ions in a solution enhances its electrical conductivity. By measuring the electrical conductivity of a solution in units of milisiemens per centimeter (mS/cm), a linear relationship can be established between the conductivity and the ionic strength expressed in terms of molarity (M). Previous research

found a linear relationship, represented in Equation 18, in solutions with an ionic strength up to approximately 39.5 mS/cm. The correlation coefficient in this study was shown to be 0.996 indicating a significant correlation (Griffin & Jurinak, 1973).

$$I = 0.0127EC - 0.0003 \qquad \text{Equation 18}$$

2.4 pH

The pH is defined as a measure of the activity of the dissolved hydrogen ions (Buck et al., 2002).

$$pH = -\log a_H \qquad \text{Equation 23}$$

$$a_H = [H^+] \cdot \gamma_H \qquad \text{Equation 24}$$

The term $[H^+]$ is the concentration protons in solution, and γ_H is the molal activity coefficient of protons.

Thus, accurate determination of pH depends on both careful establishment of the concentration of protons and its activity coefficient.

When looking at the application of the model within a photobioreactor inoculated with autotrophic microalgae, the proton concentration relies heavily on the carbon dioxide entering the solution and its uptake rate by the microalgal species (Berenguel et al., 2004). However, the concentration of protons hence medium pH can also be influenced by the uptake of a nitrogen source. In more detail, NO_3^- or NO_2^- uptake would result in the consumption of a proton whereas NH_4^+ uptake would result in the excretion of a proton (Eriksen et al., 2007).

2.5 Gas-liquid transfer of CO_2

The entering of CO_2 as a gas into the medium follows the gas-liquid mass transfer of the species into the liquid phase. As the mass transfer and diffusion from the liquid into the gas are much faster, gas-side mass transfer resistance on the gas-liquid interphase can be neglected (Ndiaye et al., 2018; Olsen et al., 2017). The mass transfer of CO_2 is described by Equation 19.

$$F_{CO_2} = k_l a (\frac{c_{CO_2.g}}{m} - c_{CO_2.l}) \qquad \text{Equation 19}$$

In this Equation, $c_{CO_2.l}$ is the CO_2 concentration in the liquid, $c_{CO_2.g}$ is the CO_2 concentration in the gas phase, $k_l a$ is the mass transfer coefficient and m is the partition coefficient for CO_2.

In the case of an ideal gas mixture, Henry's law as a function of temperature can be applied to find the partition coefficient m, as revealed in Equation 20 (Boom et al., 2021).

$$m(T) = \left(H_{CO_2}(T_{ref}) \exp\left(-\frac{\Delta_{sol}H}{R}\left(\frac{1}{T} - \frac{1}{T_{ref}} \right) \right)(RT) \right)^{-1} \qquad \text{Equation 20}$$

$H_{CO_2}(T_{ref})$ is the Henry solubility for CO_2 in water at the reference temperature 298.15K and $\Delta_{sol}H$ is defined as the enthalpy of dissolution of CO_2 in water.

The presence of dissolved salts decreases the solubility of CO_2, commonly known as the "salting out effect" (Sander, 2015). The H_{CO2} is dependent on the ionic strength of the respective medium described via the Sechenov equation (Equation 21) (Sander et al., 2022).

$$\log\left(\frac{H_0}{H}\right) = k_s \cdot I$$
Equation 21

The constant k_s is the molality-based Sechenov constant which depends on the electrolyte (e.g. NaCl) and can be found in IUPAC databases (*IUPAC-NIST Solubilities Database*).

Regarding the effect of changing salinity on $(k_l a)_{CO_2}$ values, controversial effects are reported in previous studies. It has been shown that seawater or electrolytic solutions show an increase in $(k_l a)_{CO_2}$ when comparing to tap water (Elhajj et al., 2014; Tokumura et al., 2006). However, both Barrut et al. (2012) and Moran (2010) report no effects of salinity of the water on the mass transfer rate of carbon dioxide.

An estimation of the rate of gas-liquid transfer of CO_2 is often based on a measured transfer rate of O_2 (Boogerd et al., 1990; Ifrim et al., 2014). This because measurements of CO_2 rates are challenging due to the direct formation of carbonic acid. Here, the rate of transfer of both components is related according to the following equation:

$$(k_l a)_{CO_2} = (k_l a)_{O_2} * \left(\frac{(D_L)_{CO_2}}{(D_L)_{O_2}}\right)^{0.5}$$
Equation 22

Previous research establishes the assumption of the $(k_l a)_{CO_2}$ to be 0.893 times $(k_l a)_{O_2}$ (Boogerd et al., 1990). Furthermore, the determination of the oxygen mass transfer of non-respiring systems can be done by using the static method (Galaction et al., 2004). This method relies on the increase of dissolved oxygen in the medium by aeration of the reactor after nitrogen sparging which provides an oxygen concentration of nearly zero.

3. Methods and materials

This chapter focuses on the development of the mathematical model for the simulation of the dynamic carbonate system. Furthermore, the process of calibrating and validating the model is explained, along with the details of the experimental set-up.

3.1 Mathematical model

The development of the model describing the dynamic carbonate system and the change in pH was performed in MATLAB R2020b. The input of the model consisted of off-gas CO_2 and EC data files, along with the initial conditions for each experiment. Also, measured pH data was used to initialize and calibrate the model. The model's output was a matrix of species concentrations within the carbonate system varying over time together with the estimated change in pH. Additionally, the plots of this behavior were generated, and the difference between the model predictions and the measured value was quantified.

The model was organized into separate functions and scripts, each handling different datasets or calculation systems. Data files and the starting points of each experiment were given as input within the model execution script. Subsequently, this execution script refers to the data processing function which links to the data import functions and the description of the carbonate system. Here, the import functions handle the raw EC, CO_2, and pH data. The carbonate system simulation function describes the equations required to establish species concentrations within the system. This script links to a function defining the constant parameters during the experiments. Figure 5 provides an overview of these functions, showing their respective roles and linking with other scripts.

The following assumptions were made while developing the mathematical model:
- Liquid and gas within the reactor are perfectly mixed.
- The gas phase behaves like an ideal gas.
- Temperature is constant, and it is set to $25°C$.
- There is a negligible amount of carbon dioxide present in the incoming airflow at the start of each experiment since the solution is sparged with nitrogen overnight.
- The Henry constant change is negligible during each experiment.

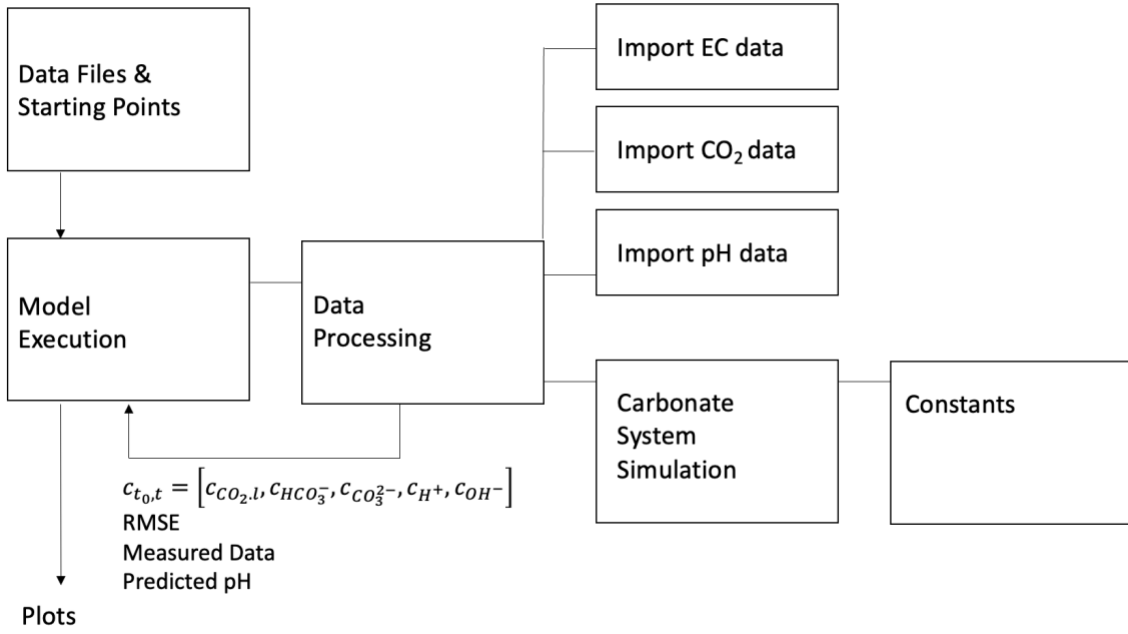Appendix 8.1 shows the complete MATLAB code written.

Figure 5. The structure of the MATLAB model that is estimating species concentrations within a carbonate system, with subsequent pH estimation over time.

To estimate the concentrations of the species present within the carbonate system, an ordinary differential equation (ODE) solver was utilized, with the respective state variables, $[CO_2]$, $[HCO_3^-]$, $[CO_3^{2-}]$, $[H^+]$ and $[OH^-]$. The data processing function referenced the specific equations required to solve the simulation within the carbonate system simulation function. Modeling the concentrations of the species relied on the dynamic CO_2 concentration in the off-gas, EC measurements converted to ionic strength, and the kinetic equations described in Chapter 2.2. Figure 6 shows the matrix resulting from solving the mathematical model of the ODE function.

$$c = \left[c_{CO_2.l}, c_{HCO_3^-}, c_{CO_3^{2-}}, c_{H^+}, c_{OH^-} \right]$$

$$c_{CO_2.l} = (k_l a)_{CO_2} \left(\frac{c_{CO_2.g}}{m} - c_{CO_2.l} \right) - \left(\frac{\gamma_{CO2.l}}{\gamma_{HCO3}\gamma_H} K_1 \frac{c_{CO_2.l}}{c_H} - c_{HCO_3} \right)$$

$$c_{HCO_3} = \left(\frac{\gamma_{CO2.l}}{\gamma_{HCO3}\gamma_H} K_1 \frac{c_{CO_2.l}}{c_H} - c_{HCO_3} \right) - \left(\frac{\gamma_{HCO3}}{\gamma_{CO3}\gamma_H} K_2 \frac{c_{HCO_3}}{c_H} - c_{CO_3} \right)$$

$$c_{CO_3} = \frac{\gamma_{HCO3}}{\gamma_{CO3}\gamma_H} K_2 \frac{c_{HCO_3}}{c_H} - c_{CO_3} \qquad \longrightarrow \qquad \frac{dc}{dt} = f\left(t, \left[c_{CO_2.l}, c_{HCO_3^-}, c_{CO_3^{2-}}, c_{H^+}, c_{OH^-} \right]' \right)$$

$$c_H = c_{HCO_3} + c_{CO_3} + c_{OH} - c_{Cation}$$

$$c_{OH} = \frac{K_w}{\gamma_{OH}\gamma_H} \frac{1}{c_H} - c_{OH}$$

Figure 6. Matrix form of the mathematical model describing the species concentration changes over time in the carbonate system.

In more detail, the MATLAB ODE solver function ode15s was used to calculate species concentrations and their change over time. This ODE function is specifically suitable for solving stiff differential equations (Shampine & Reichelt, 1997). Here, stiff differential equations are defined to be numerically unstable. Hence, small steps were required to take by the numerical method used (Garfinkel et al., 1977). This was done by the quasi-constant step size implementation of the ode15s function of MATLAB, varying the step size

of simulations within a defined tolerance. The input of this ode15s-solver required, next to the differential equations, the total simulation timespan, and an initialization of the state variables. Hence, to initialize the matrix, the pH measured at the start of the experiment was used to calculate $[H^+]$ and $[OH^-]$. Additionally, a term accounting for the surplus of cations present in the solution, the cation fit factor, was included manually.

The specific activity was required to accurately model the species concentrations. In the model, the ionic strength measurements of the medium solution are incorporated within each timestep of the ODE solver by employing the monitored EC measurements converted into ionic strength. The conversion equation, $I = 0.0127EC - 0.0003$, assured a linear relation between the EC and ionic strength of the solution, as described in more detail in Chapter 2.3. The activity coefficients of the species present were computed based on the ionic strength of the solution. If the ionic strength did not exceed 0.5M, the Davies equation gave an estimation of the activity coefficients. In solutions of higher ionic strength, the empirical relations described in Chapter 2.3 were used to compute values for the activity coefficients of the dissolved species.

With the use of the predicted proton concentration and its activity coefficient, the pH was calculated at every time point.

An additional MATLAB function was implemented to handle the constants related to the system's behavior. The constants included temperature and based on this temperature pK_1^0 and pK_2^0 values were computed. Moreover, the pressure within the bioreactor was calculated based on the overpressure measured during the experimental run. The Henry constant, which characterized the solubility of CO_2 in the solution, was calculated based on the initial ionic strength, as explained in Chapter 2.5. Lastly, the mass transfer coefficient for CO_2 ($(k_l a)_{CO_2}$) was calculated based on a measured $(k_l a)_{O_2}$, as described in Chapter 2.5.

3.1.1 Model calibration

Before applying the model to solutions with different ionic strengths, calibration was required to be performed over the range of 0.1M and ASW (~0.6M). Model calibration required data from EC, off-gas CO_2, and pH measurements. The predicted pH was fitted to the measured pH for each ionic strength solution by setting a cation fit factor. This cation fit factor was included in the electron balance, as depicted in Figure 6 by the determination of the proton concentration. By incorporating the cation fit factor, the predicted pH values could be effectively adjusted to closely match the measured pH values, assuring calibration of the model for each ionic strength solution.

The accuracy of the calibration and cation fit factor was determined based on the accuracy of the measurement data of the EC, off-gas CO_2, and pH measurements. To analyze the accuracy of these measurements, the standard deviation is analyzed and a calibration curve for the off-gas analyzer was made. This calibration curve involved measuring the off-gas CO_2 concentrations without passing through the medium, by bypassing the reactor.

3.1.2 Model validation

To verify the predictability of the cation fit factor, a validation experiment was performed. The validation aimed to assess whether the model could accurately predict the cation fit factor for a certain ionic strength of the solution within the calibration range. The accuracy

was determined by comparing the modeled pH to the measured pH during the experiment. For this, the Root Mean Square Error (RMSE) was calculated every second of the simulation. The RMSE is commonly used as the statistical metric to measure model performance, as it quantifies the error between the model predictions and the corresponding measured values in the same units (Hodson, 2022). By calculating the RMSE at every time point throughout the simulation, the model's performance could be assessed during the complete experiment. Lower RMSE values indicated a higher level of agreement between the model and the measured data, suggesting better accuracy and reliability of the model in predicting the dynamic carbonate system.

$$RMSE = \sqrt{\frac{1}{n}\sum_{i=1}^{n}(y_i - \hat{y}_i)^2}$$ Equation 23

Where, n is the number of observations, y_i is the measured value, and $\hat{y}_i$ is the corresponding model prediction.

3.2 Experimental Set-up

All calibration and validation experiments were performed in an INFORS-HT flat panel airlift photobioreactor with a working volume of 1.8L (Figure 7). The temperature was kept at a constant temperature of 25 ℃ using the heating jacket of the INFORS system. To remove water vapor from the gas phase, exhaust gas was led through a condenser and cooled to 2°C. Overpressure in the reactor was measured by a U-manometer and high overpressure built-up was prevented by a pressure safety system in the form of a water lock attached to the headspace of the bioreactor. No pressure could be built up in the reactor since a higher pressure would assure water transfer out of the tube connected. An inner pressure increase above a threshold of the maximal water column would push water and subsequently gas toward the open environment preventing reactor damages, as illustrated in Figure 8.

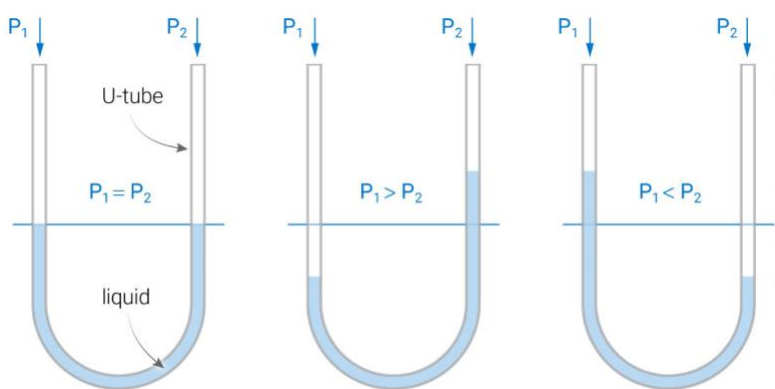*Figure 7. Labfors 5 Lux LED flat panel (Franco, 2017).*

Figure 8. Water lock controlling pressure inside the reactor.

The INFORS flat panel airlift reactor was equipped with horizontally installed sensors for pH, Dissolved Oxygen (DO), temperature, and Electrical Conductivity (EC), as presented in detail in Figure 9. The reactor holds three mass-flow controllers, which enable the adjustment of the surpassing gas flow rates. This was based on the heat capacitance of the gas they were calibrated against. The input gas flow rates were configured in mL/min units. To enhance the average gas retention time, gas recirculation was employed, as illustrated in Figure 9. This approach was followed to address the limitation of the gas analyzer, which had a maximum capacity of 200 mL/min. Moreover, the gas recirculation set up simulated a common configuration used when inoculating with microalgae to improve the efficiency of CO_2 removal within the reactor (Cuaresma et al., 2011).

The pH probe (Mettler Toledo InPro 3030) was calibrated via a two-point calibration with buffer solutions of pH 4 and pH 10. Data logging of the pH measurements occurred every 10 minutes or whenever a change in pH of 0.05 pH units was detected, with the use of the software tool Iris V5 installed on a computer coupled to the INFORS unit. Similarly, temperature measurements were logged using the same software and method as the pH measurements.

The EC probe (Mettler Toledo lnPro7001i) was a smart sensor calibrated by the supplier and with the calibration data stored within its chip. The calibration was verified at the start of each experiment using a reference standard from Mettler Toledo with a conductivity of 12.88 mS/cm. The EC data was automatically logged every 30 seconds and exported as csv file after each experiment via the Transmission Configuration Tool (TCT) supplied by Mettler Toledo.

Furthermore, an off-gas analyzer, Servomex 4100 Gas Purity Analyzer, was integrated into the reactor set-up to monitor the CO_2 and O_2 concentration in the outgoing gas. Calibration of the gas analyzer involved a two-point calibration using a calibration gas mixture (2.46% CO_2) and a pure N_2 flow for low-point calibration (0% CO_2). The off-gas analysis was logged every 5 seconds through a Labview-generated DAQ software tool which generated a text file per day.

A dissolved CO_2 probe is tested to compare the model's response on this measurement to the off-gas CO_2 analysis. The dissolved CO_2 probe (Hamilton CO_2NTROL RS485 120) was calibrated equally to the off-gas analyzer, ensuring consistency between the two

measurement methods. The measurements were logged every minute through the corresponding software tool supplied by Hamilton generating an Excel file per experiment.

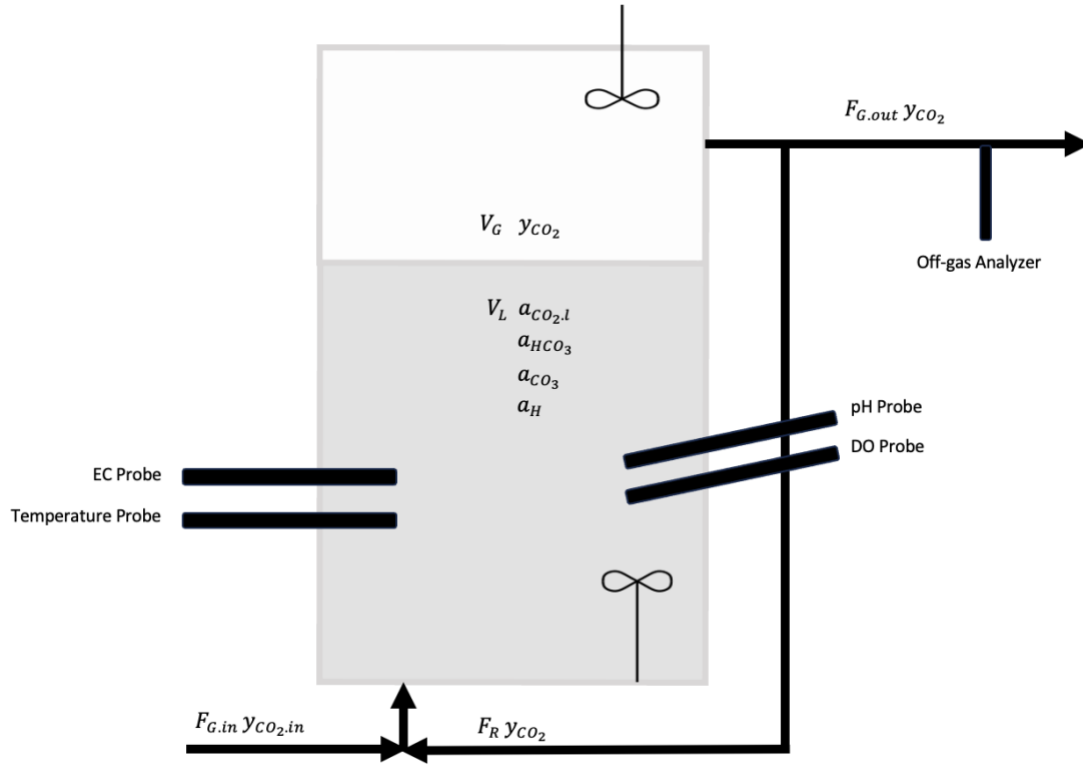The quality certificates of the probes are depicted in Appendix 8.2.

Figure 9. Reactor set-up including the position of the sensors and identification of the components in the liquid and gas phase.

3.2.1 Model calibration

Model calibration required data on the CO_2 concentration in the off-gas, EC, and pH measurements during each experiment. For the experiments, artificial seawater (ASW) was diluted to reach solutions with an ionic strength of 0.1M, 0.2M, 0.4M, and 0.5M. Lastly, undiluted ASW was used (~0.6M). The pure ASW-solution contained (per liter) 0.8 g $CaCl_2*2H_2O$, 24.5 g NaCl, 9.8 g $MgCl_2*6H_2O$, 3.2 g Na_2SO_4, and 0.85 g K_2SO_4. Experiments at each ionic strength were carried out in triplicates and started at a CO_2 concentration of 0%. Then, CO_2 concentration was increased stepwise to 1% and 2% v/v, representing 0.01 and 0.02 atm, as shown in Figure 10. At each concentration step equilibrium was awaited before the next step started. During the experiments, pH, off-gas CO_2, and EC were constantly measured. The temperature was kept constant at 25 °C using the heating jacket of the system. Measurements were performed and logged following the procedures described in Chapter 3.2.
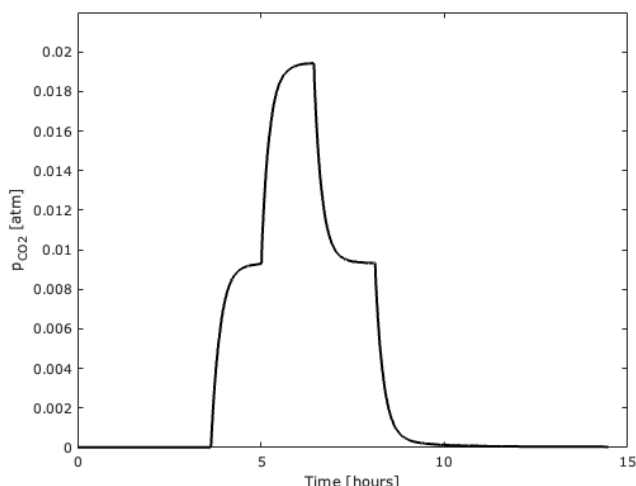
Figure 10. Change in CO$_2$ concentration (resembling pCO$_2$ in the off-gas) during each experiment.

3.2.2 Model validation

A validation experiment was carried out in duplicate. The solution used for validation was set to an ionic strength of approximately 0.3M, which fell within the range of the calibration (between 0.1M and 0.6M). Similar to the calibration experiments, variations in the CO$_2$ concentrations were set to induce changes in the pH of the solution. In order to observe if the model's predictions would follow smaller deviations in pH, the steps in CO$_2$ concentrations were set to be smaller. The CO$_2$ concentration in the gas phase was increased stepwise to 0.5%, 1%, 1.5%, and 2% v/v, with each concentration step allowing for equilibrium to be reached before proceeding to the next step. Throughout these saturation and desaturation processes, continuous monitoring of pH, EC, off-gas CO$_2$ and temperature was carried out. The temperature was maintained constant at 25 °C. Measurements were performed and logged following the procedures described in Chapter 3.2.

3.2.3 NaOH addition

Experiments were performed to see how the model reacts to the addition of sodium hydroxide (NaOH). The addition of alkaline solutions results in a change in cation concentration in the solution. To perform these experiments, the reactor medium was spiked with 0.36mL, 1.08mL, and 1.8mL of 1M NaOH solution resulting in concentrations of 0.2mM, 0.6mM, and 1mM NaOH, respectively. The experiment was conducted at a saturation concentration of 1% v/v CO$_2$. Each addition of NaOH was introduced once the system reached an equilibrium state. The reactor set-up, measurements, and data logging remained identical to those employed in the calibration and validation experiments.

4. Results and discussion

In this chapter, calibration model results are discussed, and the accuracy of this calibration will be established. Hereafter, model validation is described and reviewed.

It is relevant to note that solutions with an ionic strength lower than 0.1M are not considered due to the inaccuracy of pH sensors in these solutions. In pure water, the pH electrode tends to drift and responds slowly giving inaccurate, and non-reproducible measurements. This is due to the low conductivity of the solution since the changes in liquid junction potential and the absorption of CO_2 into the solution are minimal (Thermo Fisher Scientific, 2012).

4.1 Model calibration

The mathematical model computed results in a simulated pH based on the concentration of CO_2 in the off-gas and the EC measurements in the solution. Figure 11 shows the model responses for the first run of the triplicate experiment conducted on the solutions with an ionic strength of 0.1M, 0.2M, 0.5M, and an undiluted ASW solution. The calibration of the model involves the determination of the cation fit factor at each ionic strength. To fit the predicted pH by the model to the measured pH more correctly, the surplus of cations to anions is included in the model to account for the net positive charge present within the solution. The cation fit factor considers the positively charged components present aside from the protons. This fit factor is used to determine the proton concentration over time by including this cation concentration in the electron balance.

As depicted in the Figures 11C and 11D, when solutions contain a higher ionic strength, fitting the model exactly to the measured pH values assures difficulties. To address this challenge, two options for calibrating the model are considered. The first option fits the model to the initialization phase, where the predicted pH is set equal to the measured pH at the start of the experiment. Here, the CO_2 concentration is 0% v/v and the pH is approximately 7.5. The second option fits the model to the measured pH values when the CO_2 concentration is 1% v/v and the pH is approximately 5. In the subsequent sections, the advantages and disadvantages of both calibration options will be examined and discussed.

4.1.1 Model fit at 0% v/v CO_2 concentration

As mentioned before, Figure 11 shows the model responses for the experiments performed with solutions containing an ionic strength of 0.1M, 0.2M, 0.5M, and undiluted ASW. Here, the model is fitted to the initialization phase of the measured pH. The accuracy of the model over the complete experiment is determined by the Root Mean Square Error (RMSE). The model simulations at an ionic strength of 0.1M and 0.2M yield an average RMSE for the experiments of 0.074 and 0.203, respectively. In the case of the least diluted solution with an ionic strength of 0.5M, the RMSE is computed at 0.125. For the undiluted ASW, the RSME is 0.163.

It is relevant to mention that the experiment conducted on the solution with an ionic strength of 0.1M was performed in duplicate, while subsequent experiments starting from 0.2M were conducted in triplicate. The decision to switch to triplicate experiments was based on the realization that triplicate experiments provide the opportunity to calculate standard deviations. By having multiple replicates, it becomes possible to assess the variability and reliability of the measurements, thus providing a more robust and statistically meaningful analysis of the data.
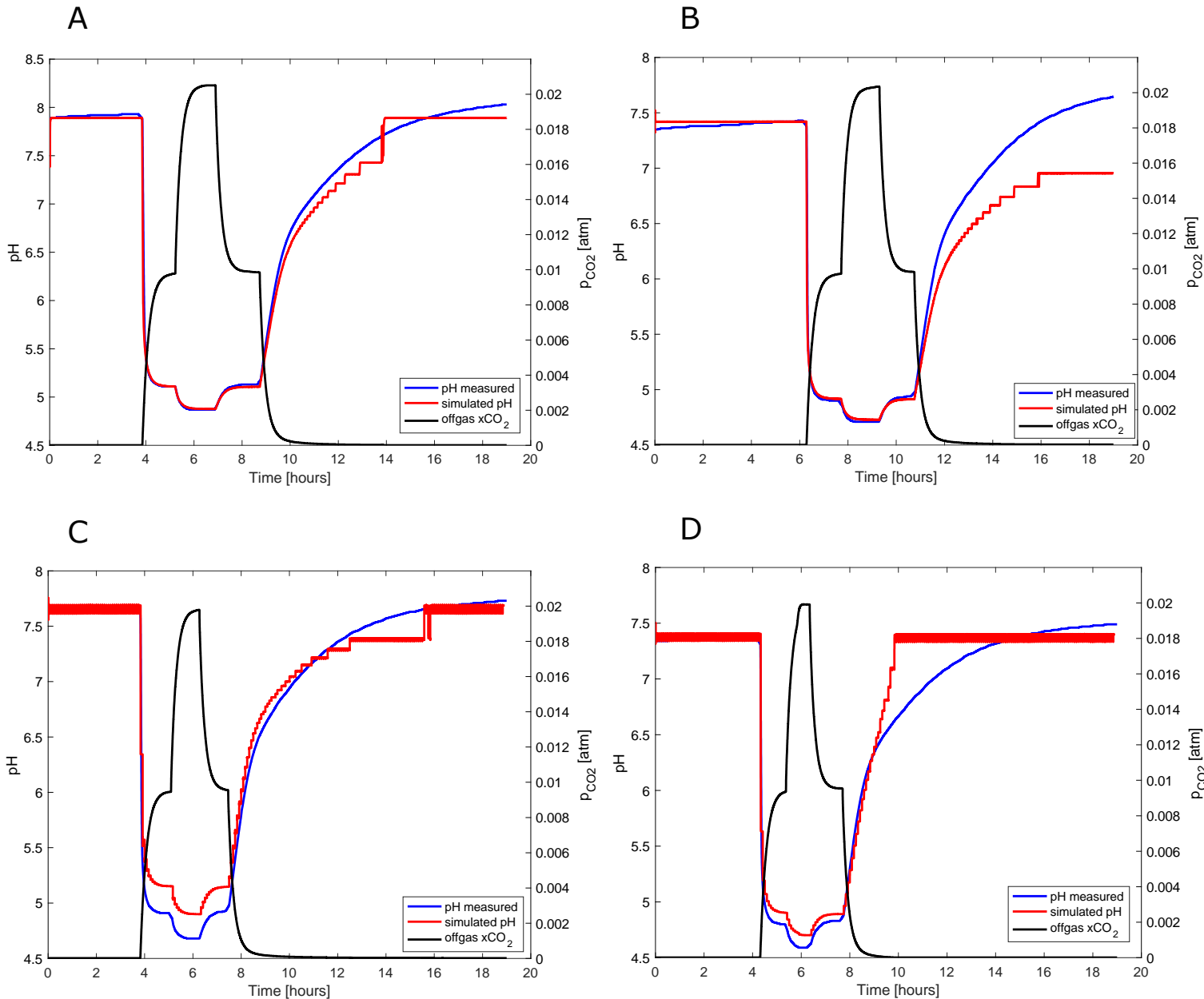

Figure 11. Model response for artificial seawater (ASW) dilutions with an ionic strength of 0.1M (A), 0.2M (B), 0.5M (C), and undiluted ASW (D) where CO_2 is stepwise changed to 1% and 2% v/v and the model cation fit factor is set to fit the measured pH during the initialization phase.

The evaluation of the model's performance based on the RMSE values indicates that the model is not able to precisely predict the measured pH. However, despite the deviations, the model response is comparable to the measured pH during the dynamic CO_2 concentrations in the different dilutions of ASW and undiluted ASW. To explain in more detail, Figure 12 illustrates the change in RMSE per calibration model response to stepwise alterations in CO_2 concentration across the artificial seawater (ASW) dilutions with an ionic strength of 0.1M, 0.2M, 0.4M, 0.5M, and undiluted ASW.

Figure 12. The calculated Root Mean Square Error (RMSE) between the model's response and the measurements during the experiments when fitting the model during the initialization phase.

The cation fit factor is influenced by the ionic strength, as illustrated in Figure 13. However, the five data points displayed in the graph do not exhibit a clear correlation. The experiments conducted on solutions with ionic strengths of 0.2M and 0.5M show a significant standard deviation, indicating large variability in the cation fit factor between the triplicates in the experiment. Furthermore, the cation fit factor values at 0.4M and in ASW (0.6M in the graph) appear to be relatively low. It is evident that more experiments and data points are required to establish a stronger correlation between the cation fit factor and the ionic strength when fitting the model response to the measured values during the initialization phase.
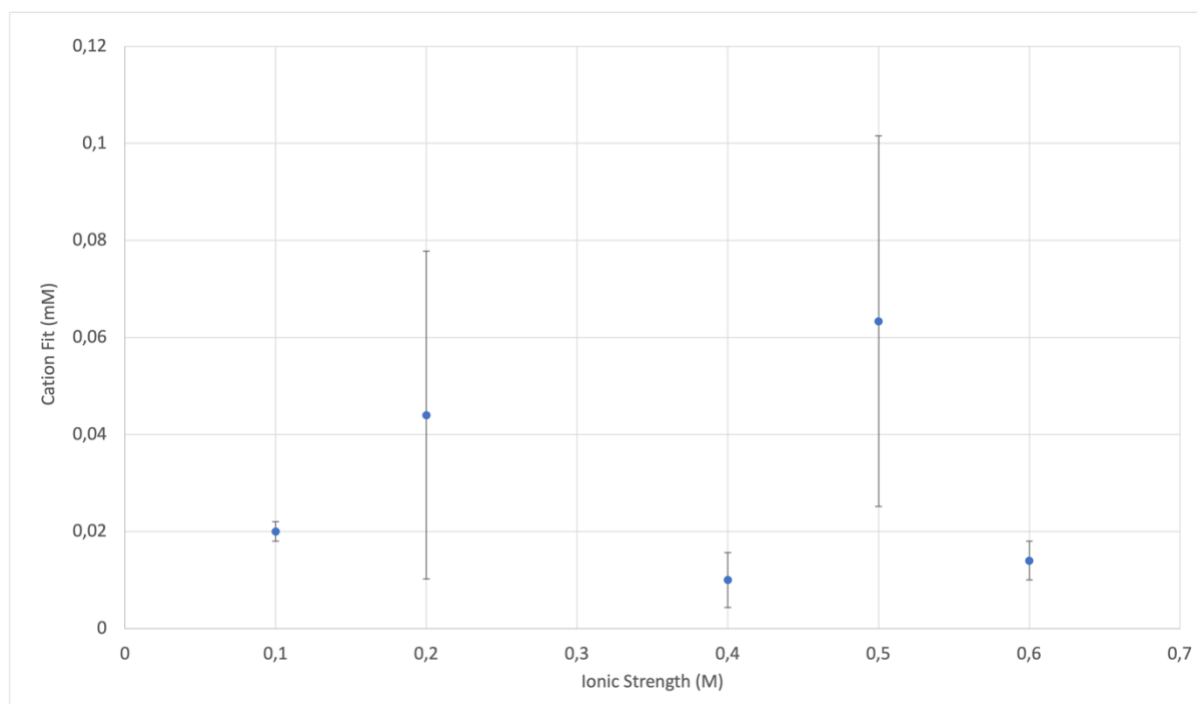
Figure 13. Cation fit factor set to fit the model's response to the measured pH values during the initialization phase.

4.1.2 Model fit at 1% v/v CO$_2$ concentration

The alternative option of fitting the model response to the measured values when the CO$_2$ concentrations reached a value of 1% v/v provides different values for the cation fit factor compared to the fitting during the initialization phase. For the experiments conducted on the 0.1M and 0.2M solutions, this alternative fitting option assure no significant difference in the RMSE of the experiments. However, for solution with higher ionic strengths, notable differences are observed. Figure 14 presents the model responses for the ASW dilutions with an ionic strength of 0.1M, 0.2M, 0.5M, and undiluted ASW when fitted at a CO$_2$ concentration of 1% v/v. The average RMSE values for the triplicate experiments for the solutions with an ionic strength of 0.1M and 0.2M are 0.074 and 0.271, respectively. In the case of the least diluted solution with an ionic strength of 0.5M, the computed RMSE is 0.515, while for undiluted ASW, the RSME is 0.216. Figure 15 further illustrates the change in RMSE per model response to stepwise alterations in CO$_2$ concentration across the artificial seawater (ASW) dilutions with an ionic strength of 0.1M, 0.4M, 0.5M, and undiluted ASW. The relatively high RMSE values indicate the presence of modeling difficulties and reduced accuracy, particularly in highly concentrated salt solutions. This highlights the challenges associated with accurately predicting the pH in solutions with a high ionic strength.

Figure 14. Model response for artificial seawater (ASW) dilutions with an ionic strength of 0.1M (A), 0.2M (B), 0.5M (C), and undiluted ASW (D) where CO$_2$ is stepwise changed to 1% and 2% v/v and the model cation fit factor is set to fit the measured pH at 1% v/v CO$_2$ concentration.
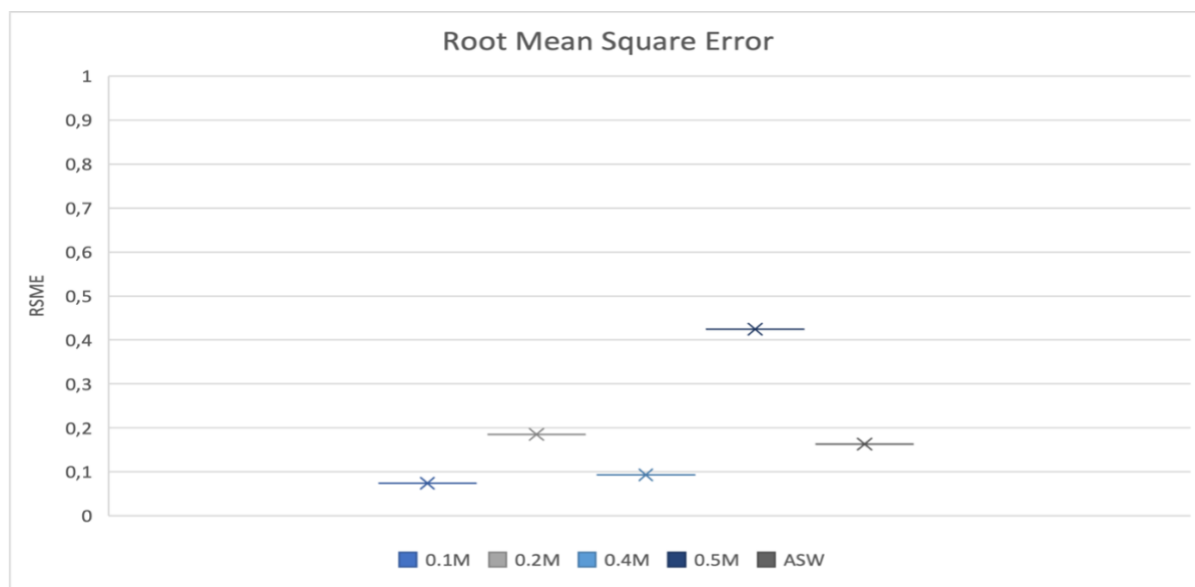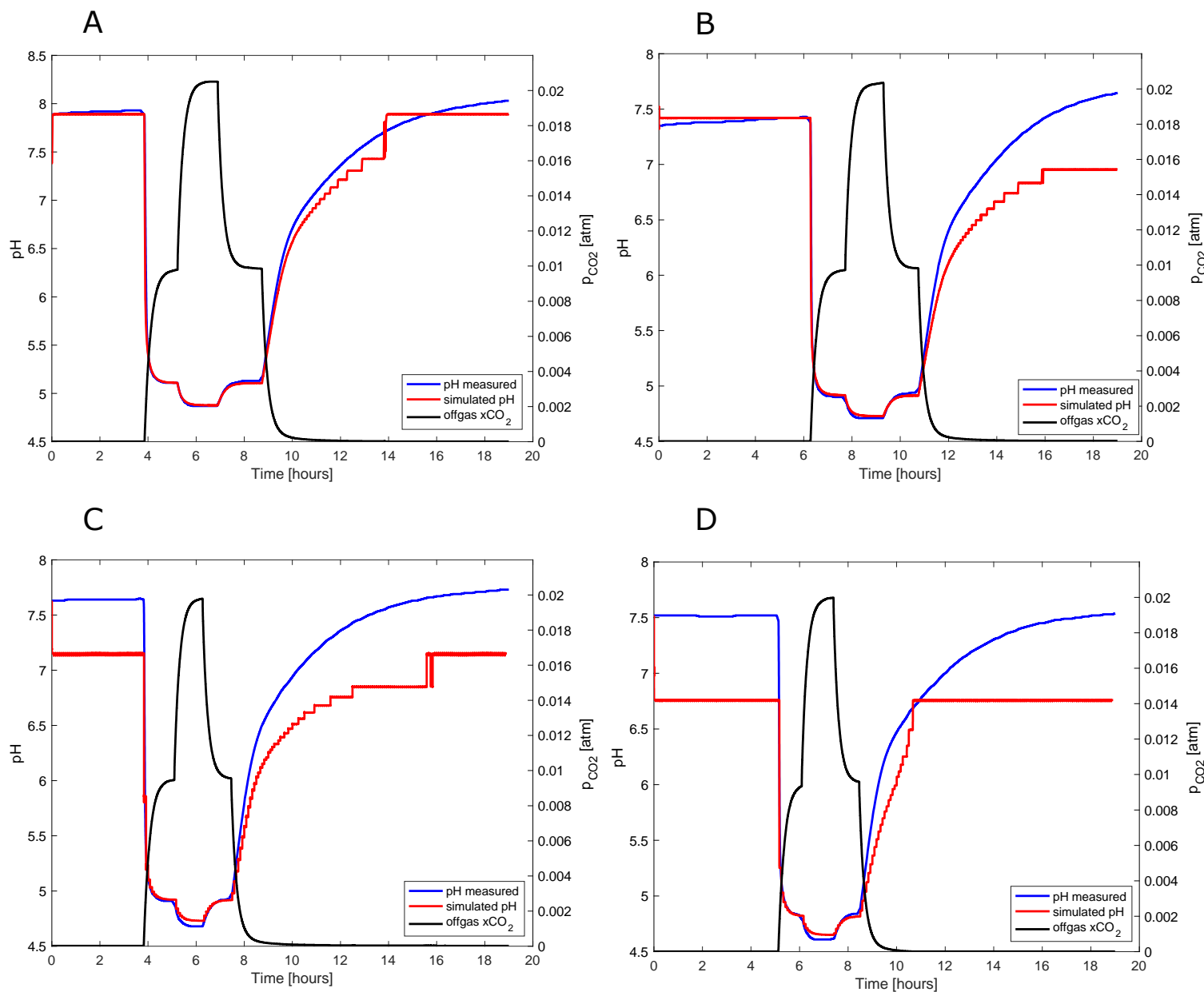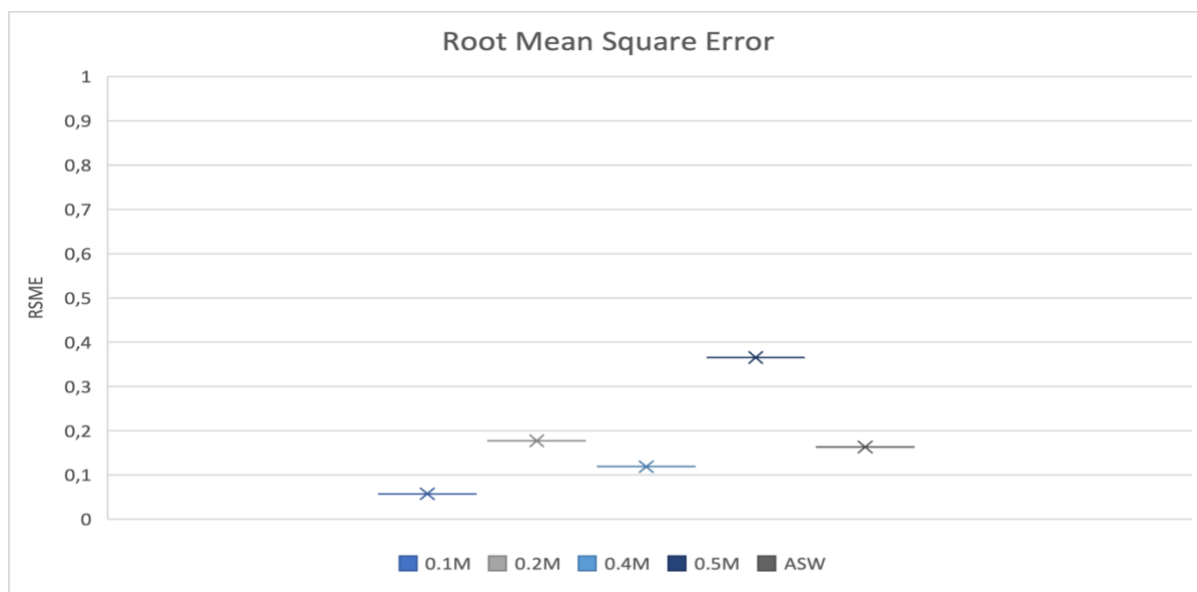
Figure 15. The calculated Root Mean Square Error (RMSE) between the model's response and the measurements during the experiments when fitting the model at a CO_2 concentration of 1% v/v.

The cation fit factor when fitting at a CO_2 concentration of 1% v/v decreases as the ionic strength of the solution increases, as depicted in Figure 16. Here, a correlation is found between the concentration cations used to fit the model and the ionic strength of the solution in which the carbonate system is assessed by the model. The relationship between the cation concentration and the ionic strength can be characterized by the equation $y = -0.0253x + 0.0213$, where y represents the cation concentration and x the ionic strength. The correlation coefficient (R^2) of 0.87 indicates a moderate relationship between the two variables. However, it is important to note that there is a relatively high standard deviation observed in the solution with an ionic strength of 0.2M. It suggests that other parameters may also be influencing the cation concentration, leading to increased variability in the data.

Figure 16. Cation fit factor set to fit the model's response to the measured values when the CO_2 concentration is 1% v/v.

29

4.1.3 Discussion on the general model's response

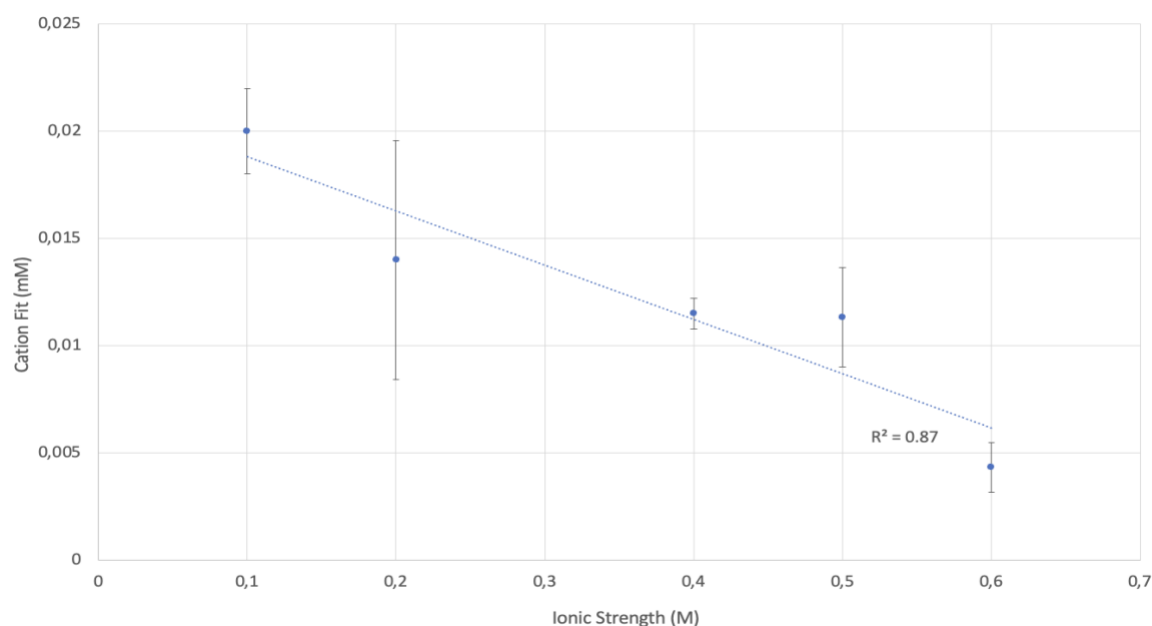Figures 11 and 14 illustrate that the model's response is comparable to the measured pH during the changing CO_2 concentrations in the different dilutions of ASW and undiluted ASW. In general, when the CO_2 concentration increases to 1% v/v, the pH drops from approximately 7.5 to 5. Moreover, when increasing the CO_2 further to 2% a further decrease in pH is observed as more protons, bicarbonate, and carbonate ions are formed. The model predicts this dynamic nature between the CO_2 concentrations and the pH similar to the measured response to the dynamic CO_2 behavior. However, certain remarks can be made regarding its behavior. Specifically, when CO_2 concentrations approach 0% v/v during the desaturation of the solution, a stepwise result of the modeled pH is obtained. It is important to consider that the off-gas analyzer has a resolution of 0.001% v/v, so CO_2 concentrations lower than this threshold will not be detected. Consequently, when reaching this lowest limit certain inaccuracies in the measurements arise. Therefore, approaching this minimum threshold of the off-gas analyzer gives a reason for the stepwise response of the model in the desaturation phase. The concentration of CO_2 is one of the main model inputs by which pH estimation is computed. That is why, when lowering the CO_2 to 0% v/v, measurements of CO_2 will decrease in steps of 0.001% v/v resulting in a stepwise response of the model. To correct partially the inaccuracies of the off-gas analyzer around 0% v/v CO_2, an adjustment to its measurements is added to the model. Particularly, any concentration of CO_2 reaching 0.003%, lower values than 0.003%, or negative values are set to 0.001% yielding a correction for the off-set of the off-gas analyzer. Explaining the bigger jump in the computed pH in the latter part of the desaturation phase, while disregarding the fluctuations of the measurements between 0.004 to 0.002% v/v. The off-set of the analyzer may be attributed to factors such as pressure difference or the presence of water vapor in the line entering the analyzer. The calibration with the use of the dry baseline described before does not account for the water vapor present or the pressure that may build up in the reactor. These factors can potentially affect the accuracy of the measurement device, leading to the need for correction.

Another observation could be made when comparing the saturation phase to the desaturation phase in the experiments. The model encounters difficulties in modeling the gradual increase in pH when the CO_2 concentration drops down to 0% v/v. While this can be partly attributed to the resolution limitations of the off-gas analyzer, there is another explanation to consider. This plausible explanation for the deviation of the model is the formation of calcium carbonate within the solution. Even in the experiments with the lowest ionic strength solution (0.1M), the model calculates 3.17E-9 M carbonate ions at a CO_2 concentration of 2% v/v. Additionally, approximately 0.04M calcium ions are present in this solution. Considering the solubility product constant of 3.36E-9 at 25 ℃ (Haynes, 2010) and the solubility reaction shown below, even in the experiments with the lowest ionic strength solutions, a 0.03M calcium carbonate could be formed.

$$CaCO_3 \ (s) \leftrightarrow Ca^2 \ (aq) + CO_3^{2-} (aq)$$
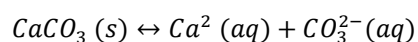
The formation of calcium carbonate at low pH results in increased CO_2 uptake by the solution to maintain the CO_2 concentration at 1 or 2% v/v. This process releases protons, leading to the formation of more bicarbonate and carbonate ions. As a result, lower pH values are measured compared to the model predictions. Conversely, during the decrease in CO_2 concentration, calcium carbonate undergoes a reverse reaction forming carbon

dioxide, eventually leaving the system. This explains the higher pH measurements compared to the model predictions, as a larger amount of CO_2 needs to be released from the solution, taking up protons in the process. This reaction of calcium carbonate formation and its redissolution and currently not accounted for in the model. It may contribute to the discrepancy between the model predictions and the experimental observations. Especially, in the experiments conducted on solutions with higher ionic strengths.

Moreover, when looking at Figures 11 and 14, it could be concluded that the pH of the solution lowers when its ionic strength increases. Starting at a pH of 7.9 in the 0.1M solution, pH lowers to 4.9 when CO_2 v/v jumps from 0% to 2%. Whereas in the 0.4M solution, a decrease in pH from approximately 7.2 to 4.7 is seen. However, a higher pH would be expected since pH is defined as a logarithmic function of hydrogen ion activity. The decrease in activity coefficient observed in more saline solutions leads to higher pH values. Therefore, it becomes necessary to identify additional factors that could account for this behavior. One potential explanation is the uncertainty associated with the pH probe used, which has an inaccuracy factor of 0.25 pH units at a pH of 7 as shown in the quality certificate in Appendix 8.2.1. Furthermore, looking at the triplicate results for the 0.5M solution pH drift is revealed, as depicted by the higher initial value of the measured pH during each experiment in Figure 17. This observed increase in pH could be due to the concentration of CO_2 in the solution. Despite the reactor being sparged with nitrogen overnight prior to the experiment, traces of CO_2 may still persist. However, after a period of 3 days, more complete removal of CO_2 is achieved, resulting in a higher pH compared to the initial pH value. It is important to note that the off-gas analyzer has an accuracy of 0.001% v/v, so CO_2 concentrations lower than this threshold will not be detected. Another explanation for this drift in pH can be related to the calcium carbonate kinetics mentioned before. Here, after each experiment, more CO_2 would leave the system, as calcium carbonate formation results in an increased CO_2 uptake. Eventually, during the desaturation phase, this would result in an increase in the measured pH. In the case of the triplicate experiments where the same solution was repeatedly used, it is plausible that the second experiment starts at a higher pH than the first experiment. This can be attributed to the residual effects of the previous experiment, contributing to the observed drift in pH.
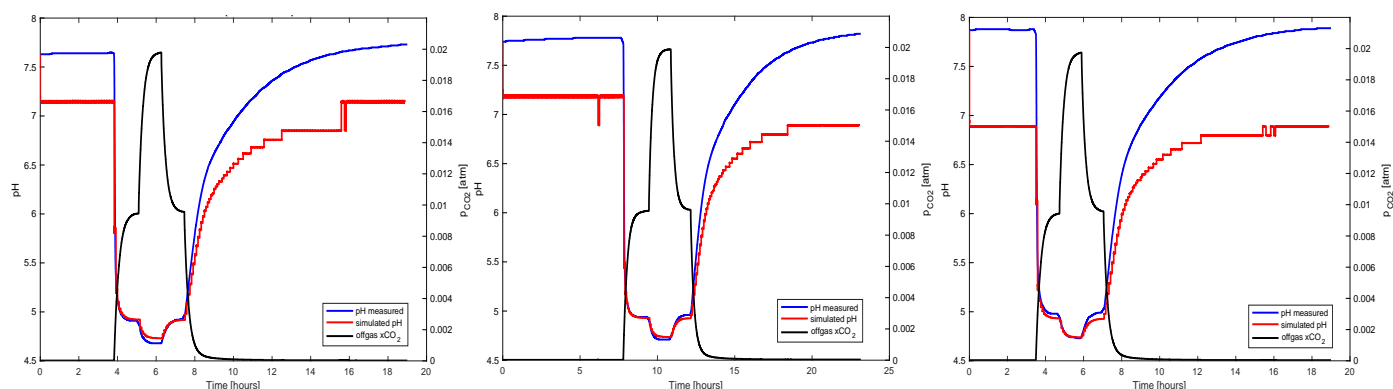

Figure 17. Stepwise CO_2 change in 0.5M solution performed in triplicate showing measured pH, off-gas CO_2 concentration and model response.

4.1.4 Discussion on the cation fit factor

The results described in Chapter 4.1.1 and 4.1.2, consider the possibility of two options for implementation of the cation fit factor. The two options, fitting the model during the initialization phase and fitting at a CO_2 concentration of 1% v/v, have both advantages and disadvantages.

Fitting the model during the initialization approach allows for convenient application to new experiments. Moreover, fitting the model's response to the measured pH values around a pH of 7, involves a low proton concentration gaining a more accurate fit. However, this approach introduces an uncertainty term due to the off-gas CO_2 measurement when approaching a concentration of 0% v/v. In the model the data in this range is processed and corrected for an off-set. Fitting the model to processed data of the off-gas CO_2 may inadequately influence the accuracy of the model's response. On the other hand, fitting the model at a CO_2 concentration of 1% v/v avoids this issue and ensures a more accurate representation of the CO_2 concentration as an input of the model. However, a drawback of modeling at higher CO_2 concentrations is that the model is fitted at lower pH values. Lower pH values correspond to higher proton concentrations on a logarithmic scale. Thus, a small difference between the model's response and the measured pH value in the lower pH regime might account for a greater difference if pH increases again.

Regarding the relationship between the cation fit factor, the surplus in cations in solution, and the ionic strength, speculations can be made. In less diluted solutions of ASW higher concentrations of K^+, Mg^{2+}. Ca^{2+}, and Na^+ cations are present. The model includes an electron balance which determines the concentration of protons in solution while considering the concentrations of the species in the carbonate system, being $[CO_2]$, $[HCO_3^-]$, $[CO_3^{2-}]$, and $[OH^-]$. Also, the cation fit factor is incorporated into this electron balance. In less diluted ASW solutions, it is expected that the surplus of cations, the cation fit factor, would be higher than in more diluted solutions. This accounts for the higher concentrations of cations present in the ASW.

Interestingly, when fitting the model's response at a CO_2 concentration of 1% v/v, a decrease in the cation concentration is observed, which contradicts this expected effect. Fitting during the initialization phase may provide better agreement, although the limited number of data points does not give a significant answer to this discrepancy.

4.1.5 Model parameters

There are multiple parameters used in the model to estimate the ion concentrations within the carbonate system. The ionic strength-dependent parameters computed by the model are the Henry constant, activity coefficients, and the equilibrium constants K_1 and K_2. Table 3 shows the ionic strength-dependent parameters calculated by the model.

The Sechenov equation described in Chapter 2.5 ensures an increase in the Henry constant when salinity increases. Here, the reference Henry constant ($H_0 = 0.033\ mol\ L^{-1}\ bar^{-1}$) at 298.15K and atmospheric pressure for carbon dioxide is used. The increase can be explained by the salting-out effect, reasoning the lower solubility of gas when the salinity of a solution increases.

As described deliberately in Chapter 2.3, the result of an increase in ionic strength of a solution is a decrease in activity coefficients of the ions in solution. The model calculates the activity coefficients of the ions in a solution based on the Davies equation or the previously described empirical-based equations. The Davies equation correlates the ionic strength and activity coefficients adequate until an ionic strength of 0.5M is reached. When the ionic strength of the solution exceeds 0.5M, the empirical relations are used to compute activity coefficients.

The equilibrium constants computed in the model are based on the relationship between salinity and the values for pK_1 or pK_2 as described by Millero et al. (2006) in Chapter 2.2. This relationship established accounts for the activities of the species within the carbonate system, which effectively takes the ionic strength into account when determining the equilibrium constants. Therefore, the use of the relationship established by Millero et al. (2006) for pK_1 or pK_2, which already considers concentrations of species, would result in double accounting for the ionic strength. To correct for this double accounting, the equilibrium constants are adjusted using the activity coefficients of the respective ions, as shown in Equations 24 and 25.

$$K_1 = \frac{\gamma_H \gamma_{HCO_3}}{\gamma_{CO_2} a_{H_2O}} 10^{-pK_1} \qquad\qquad \text{Equation 24}$$

$$K_2 = \frac{\gamma_H \gamma_{CO_3}}{\gamma_{HCO_3}} 10^{-pK_2} \qquad\qquad \text{Equation 25}$$

The final parameter used in the model to compute the dynamic concentrations of the species within the carbonate system is the mass transfer coefficient of CO_2, $(k_l a)_{CO_2}$. The estimation of the rate of gas-liquid transfer of CO_2 is based on a measured transfer rate of O_2. This $(k_l a)_{O_2}$ was measured to be 0.032 s^{-1} in the solution with an ionic strength of 0.1M. Considering their relation described in Chapter 2.5, the mass transfer coefficient of CO_2 was found to be 0.28 s^{-1}.

Table 3. Ionic strength-dependent parameters computed by the model for solutions with an ionic strength of 0.1M, 0.2M, and 0.4M.

Ionic Strength I [M]	Henry Constant H_{CO_2} [mol/L/bar]	Equilibrium Constant K_1	Equilibrium Constant K_2	Activity coefficient γ_H
0.1	0.0337	5.49E-7	1.12E-10	0.79
0.2	0.0344	6.46E-7	1.38E-10	0.76
0.4	0.0358	8.12E-7	1.69E-10	0.76
0.5	0.0366	5.12E-7	4.79E-11	0.70
Undiluted ASW ($I \approx 0.6$)	0.0378	5.19E-7	4.77E-11	0.71

4.2 Accuracy of the Measurements

As described above, measurement inaccuracies play a big role in the model response. The calibration of the model is based on measured pH, EC, and CO_2 concentration values throughout the experiments. Logically, perfect measurements are not existing hence an inaccuracy factor needs to be determined. For the off-gas analysis of CO_2, a dry baseline is used to correct the measurement errors. The dry baseline involves measuring the off-gas CO_2 concentrations without passing through the medium, by bypassing the reactor. This results in a calibration curve for the measured concentrations of 0, 1, and 2% CO_2. The dry baseline, $y = 0.973x$ with a $R^2 = 0.998$, is subsequently used to correct the wet baseline measurements during the experiments. Here, x equalizes the measured CO_2 concentration and y the corrected CO_2 concentration used further in the model.

Regarding the pH measurements, considerable differences between the initial pH in triplicate experiments executed have been found, as described before and seen in Figure 17. To quantify the differences, standard deviations (σ) of the pH measurements are calculated and plotted. Figure 18 shows the standard deviation over the triplicates of the solutions with an ionic strength of 0.2M. Especially, at the start of the experiments at the initial concentration of CO_2 (i.e., 0% v/v) a large σ is found. The mean of the σ in this experiment was 0.1165. The significant deviation at the start of the experiments can be devoted to the logarithmic relationship between pH and the proton concentrations. Higher pH values correspond to lower proton concentrations, while lower pH values correspond to higher proton concentrations. This logarithmic relationship amplifies the impact of small variations in proton concentrations, leading to larger differences in pH differences. Furthermore, the relatively high differences in the pH measurements can be caused by the 2-point calibration done at pH 4 and pH 10. To gain maximum consistency and minimum uncertainty, multi-point calibrations are recommended (Naumann et al., 2002). However, the Labfors bioreactor software used did not provide this possibility.
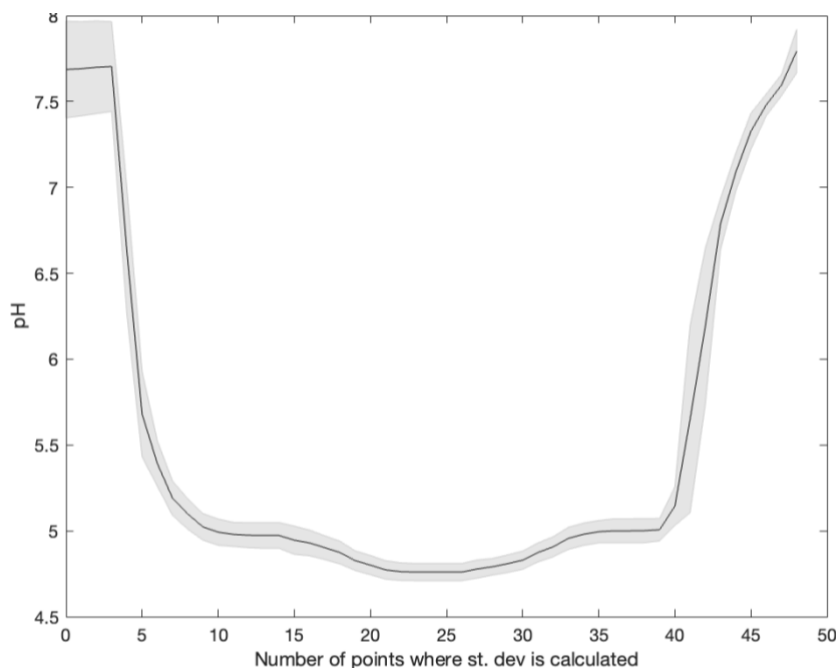
Figure 18. Standard deviation (σ) of the measured pH in a diluted ASW solution (I = 0.2M).

Next to the off-gas CO_2 measurement, the model input is based on the EC measurements within the reactor. These EC measurements show a considerable noise result during the experiment, suggesting that the measurements fall within the error range of the probe. Figure 19A illustrates the raw measurements obtained during the triplicate experiment with an ionic strength of approximately 0.5M. To enhance the clarity of the data, MATLAB R2020b was used, providing a function to smoothen the measurements resulting in Figure 19B. This smoothening function applies a moving average to the vector of measurement data while using a fixed window length. Based on these results, it can be concluded no significant difference in ionic strength is observed throughout the experiments.

Figure 19. Ionic strength measurements during the triplicate experiment in a solution with an ionic strenght of approximately 0.5M.

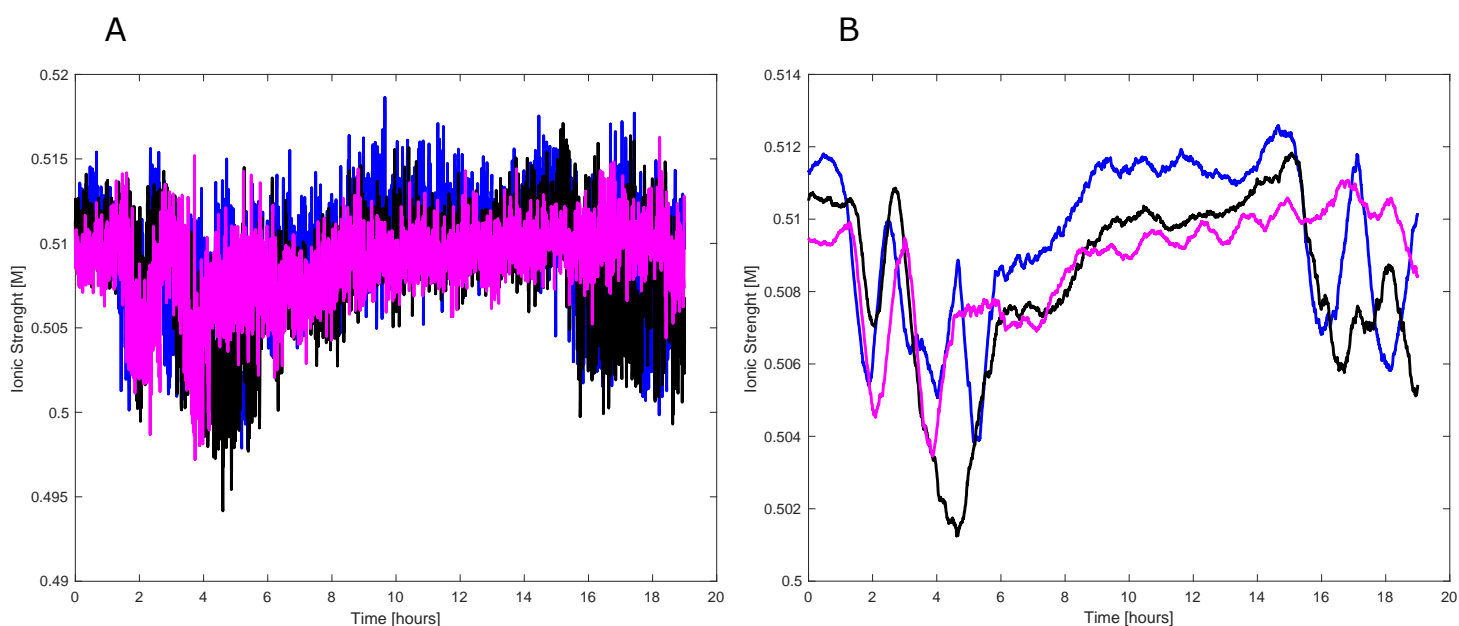Since ionic strength measurements are not significantly changing and within the error range of the probe, the model could determine the concentrations of ions present in the carbonate system solely on initialization of the ionic strength by a start value. For instance, in the triplicate experiment conducted with an ionic strength of 0.5M, the average Root Mean Squared Error (RMSE) is found to be 0.484. When the EC measurements are excluded as input in the model, the average RMSE changes slightly to 0.481, indicating that leaving out the sensor has a minimal impact on the model accuracy. To exclude EC data in the model, the ionic strength is calculated dynamically within the model itself. This is achieved by using the computed ion concentrations, allowing for the dynamic calculation of the ionic strength and subsequently, the activity coefficients. The exclusion of EC data can be advantageous in situations where permanent EC measurements are not feasible or where the measurements would be significantly influenced by other factors.

Despite the fact that excluding EC measurements may not yield a marginally different model prediction, software sensors, and their mathematical model are more reliable with multiple input variables. Incorporating data from multiple sensors enables the model to respond quickly to significant changes, leading to improved prediction accuracy improvement. Additionally, employing multiple sensors allows for the detection of potential sensor failures when any of the sensors would deteriorate (Kadlec et al., 2009). Nevertheless, challenges may arise when applying the model to microalgae photobioreactors, particularly, in measuring the electrical conductivity of the medium. The presence of microbial aggregates can interfere with conductivity due to their ability to conduct electrical current (Caizán-Juanarena et al., 2020; Li et al., 2017).

4.2.1 Dissolved CO_2 Measurements

To assess the potential for improved accuracy of the CO_2 measurements, a dissolved CO_2 probe was tested as an alternative to off-gas analysis. The goal was to determine whether measuring the CO_2 directly in the liquid would yield a more precise or comparable result of the model estimation than based on the off-gas analysis. This alternative measurement method could be particularly relevant in situations where implementing off-gas CO_2 analysis is not feasible or practical, such as during the cultivation of microalgae in an open pond.

The findings, depicted by the black line in Figure 20, reveal a relatively noisy signal when measuring CO_2 concentrations approaching 0% v/v. The presence of noise introduces significant fluctuations in the data, which has a noticeable impact on the model's response. Besides the noise in the measurements, higher concentrations of dissolved CO_2 are measured when the solution approaches an 0% v/v CO_2 concentration compared to the CO_2 measurements obtained through the off-gas analysis. As a result, the model response predicts a lower pH than the pH measured at a CO_2 around 0% v/v. The noise in the raw data could indicate that the measurements from the dissolved CO_2 probe would benefit from smoothening techniques. However, the predicted pH will remain lower than the measured pH due to the higher CO_2 concentration measured. Even though, smoothening of the data would result in less fluctuating predicted pH.

When comparing Figure 20 to Figure 11B, which both represent the same solution with an ionic strength of 0.4M undergoing stepwise changes of CO_2, a substantial difference in the model's response is observed. The use of data from the dissolved CO_2 probe resulted in an RMSE of 0.521, indicating a relatively higher level of inaccuracy. In contrast, when

utilizing off-gas analysis as an input, the RMSE was significantly reduced to 0.101, indicating a higher level of accuracy in the model's prediction.

To address the inaccuracy caused by the higher CO_2 concentration off-set at 0% v/v, a potential solution is to incorporate a data correction factor for this off-set in the model. Currently, the data of the off-gas analyzer is corrected when the CO_2 concentration reaches a value of 0.003%. Increasing this off-set correction value when using the dissolved CO_2 probe could potentially lead to a more representative and accurate result of the model's response.
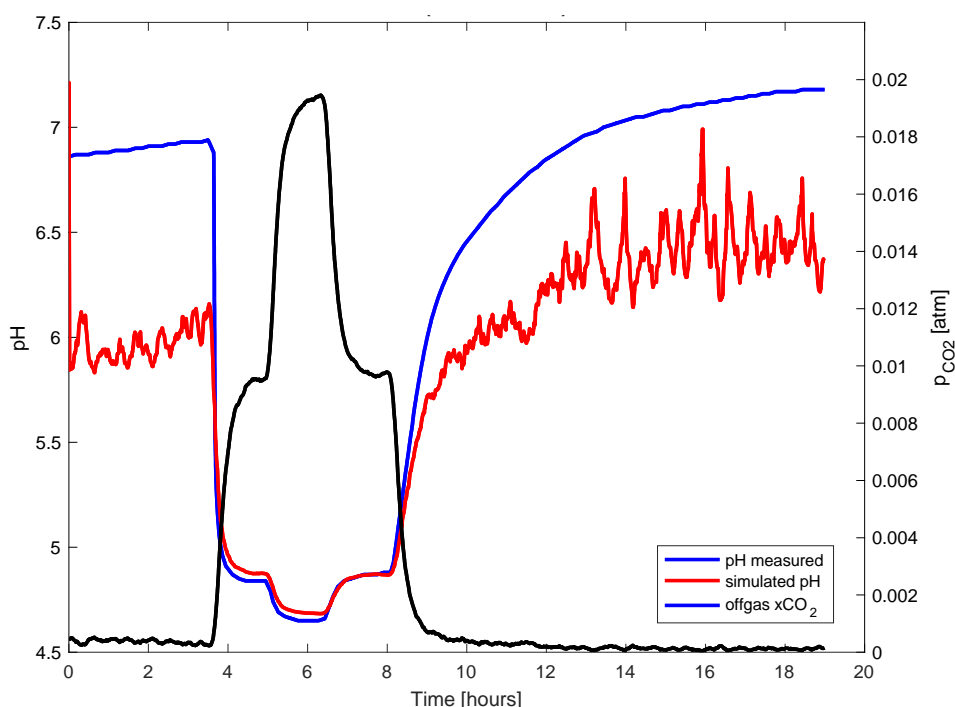

Figure 20. Stepwise CO_2 change in 0.4M solution showing measured pH, dissolved CO_2 concentration, and model response.

4.3 Model Validation

Following the calibration of the model, a validation experiment was carried out in duplicate to assess its performance. This experiment involved stepwise changing the CO_2 concentration in a solution with an ionic strength of 0.3M. The validation process applies a cation fit factor based on the established correlation between the cation concentration and the ionic strength of the solution. The selected cation fit factor of the model's response was fitted to 1% v/v CO_2 concentration, as this approach assured a linear correlation. This correlation was characterized in the calibration experiments by the equation $y = -0.0253x + 0.0213$, where y represents the cation concentration and x the ionic strength. Consequently, in a solution with an ionic strength of 0.3M the cation concentration is derived to be 0.0137M.

Figure 21 displays the results and RMSE of the second validation experiment. It can be observed that the model follows the behavior of the measurements, although the pH is predicted consistently with underestimated values. This suggest that the predicted cation was too low, leading to lower pH predictions.

The duplicate results obtained from the validation experiment show an average RMSE of 0.582 and 0.314, respectively. Figure 21 illustrates the outcomes of the second run, which exhibited slightly improved accuracy compared to the initial run. Nevertheless, over both runs a relatively low accuracy was achieved. This is attributable to several possible factors. Firstly, the software utilized for the calibration experiments experienced a crash requiring the use of an alternative infors unit for the validation experiments. Additionally, the crash may have been triggered by a defective pH probe, asking for the substitution of the pH probe for the validation experiment. This alternative use of hardware might cause deviating measurements of the off-gas CO_2 concentration and the pH of the solution. Thus, requiring a different fit factor than established in the calibration experiments.
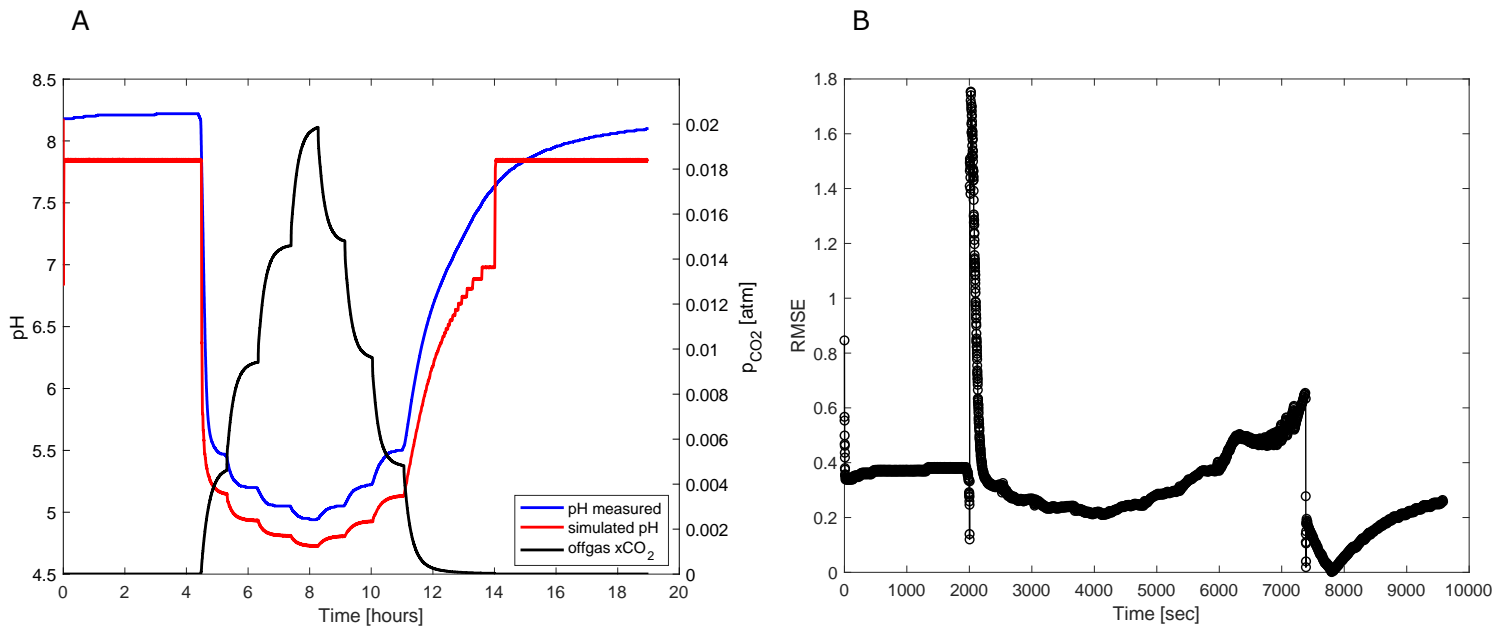

Figure 21. Stepwise change of CO_2 in a solution with an ionic strength of 0.3M, showing measured pH, CO_2 concentration in the off-gas, and simulated pH (A). The Root Mean Square Error (RMSE) of the model estimation compared to the measured pH (B).
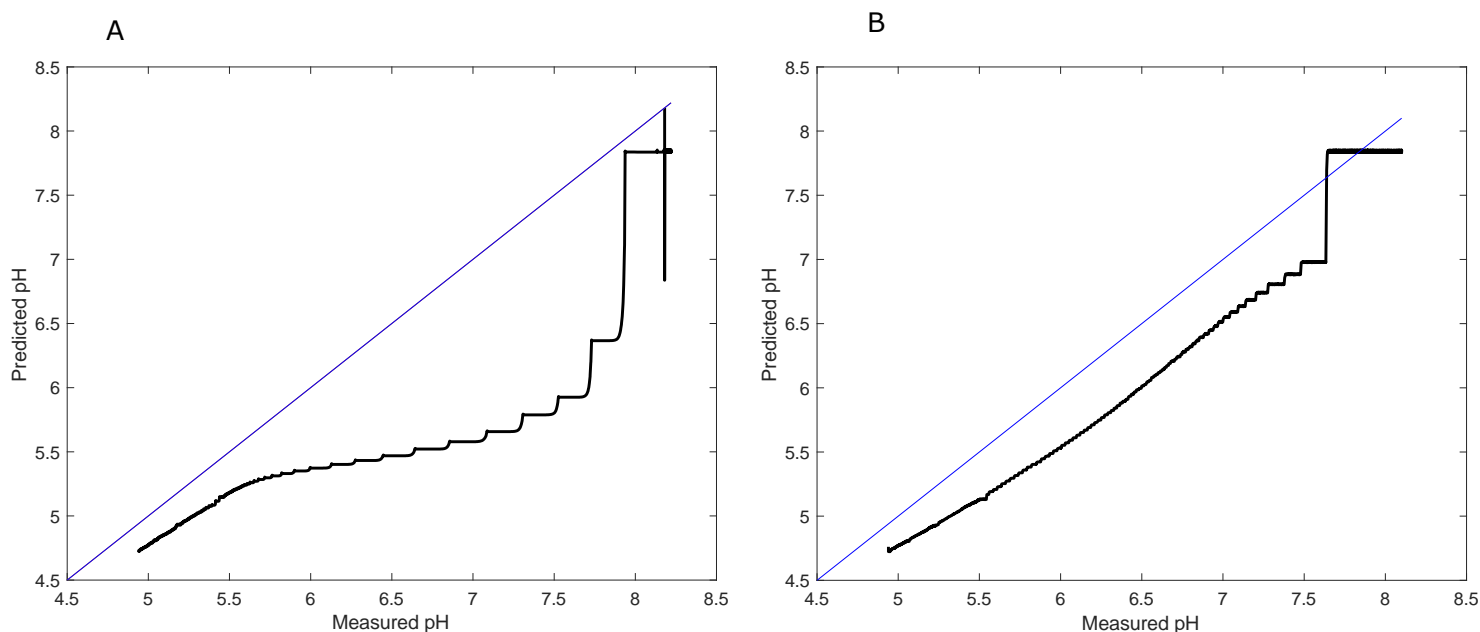
Figure 22. Difference in predicted and measured pH during the saturation phase (A) and desaturation phase (B) in a solution with an ionic strength of 0.3M.

Figure 22 provides an additional visualization, next to the RMSE, of the difference between the measured and predicted pH during the validation experiment. In Figure 22A, representing the stepwise saturation phase to 2% v/v CO_2, a constant deviation is observed at the start of the experiment, which gradually increases as pH decreases and CO_2 concentration increases. When a pH of approximately 5 is reached at a CO_2 concentration of 2% v/v, a steady deviation is shown. The diagonal line in the plot represents a perfect prediction of the measurement values, indicating no discrepancy in the model's performance.

During the desaturation phase, shown in Figure 22B, the model exhibits a relatively constant deviation, except in the last part when the pH reaches 8 and CO_2 concentration is almost 0% v/v. At this point, a jump is seen in the model deviation. Figure 22 provides a different perspective on the model's performance compared to the RMSE shown in Figure 21B. Nevertheless, the results of both graphs align, showing a relatively constant deviation except during the first drop in pH and during the last part of desaturation.

4.4 NaOH addition results

When sodium hydroxide (NaOH) is added to a solution containing dissolved CO_2, it induces a change in the cation concentration. The response of the model to this increasing cation concentration is evaluated. However, challenges arise in accurately obtaining the model's response, as shown in Figure 23B through the RMSE of the model's performance over time.

At first, the model is initialized matching its predicted pH to the measured pH in the solution. The increase in CO_2 concentration to 2% v/v shows a decrease in the measured pH to 5.2. The first addition of 0.002 M NaOH results in an increase in measured pH. The model, however, responds with a higher pH of 6.0 to the CO_2 increase and deviates to the measured pH after NaOH addition as well, as illustrated in Figure 23A. Subsequent NaOH

additions result in an underestimation of the pH. The average RMSE for this experiment, conducted in a solution with an ionic strength of 0.5M and a fixed concentration of 0.5% v/v CO_2, was 0.233.

Figure 24 presents the change in ionic strength during the experiment. As Na^+ and OH^- ions are added step wise, an increase in ionic strength during these additions would be expected. However, while the start and end measurements of the ionic strength show an increase, no clear stepwise increase is observed. Furthermore, the continuous increase of the measured ionic strength can not be explained. A plausible factor reasoning the measurements detected, might be justified by the small increase of ionic strength, which is approximately only 0.01 mS/cm. Such a small change may indicate that the measurement differences fall within the error range of the probe, leading to the lack of clear stepwise increase in the ionic strength data.

It is important to note that the accurate timing of the NaOH addition is crucial when modeling this experiment. The incorrect time setting of NaOH addition leads to unreliable changes in the ion concentrations, of both the cation and hydroxide ions, in the model's predictions. This results in an inaccurate response of the proton concentration and an unrealistic pH of 15. The precise timing of the NaOH addition is essential to ensure an appropriate CO_2 buffer capacity at the moment of the hydroxide introduction. Thus, when the CO_2 concentration declines, the addition of the hydroxide ensures a decrease in the proton concentration, subsequently lowering the pH.
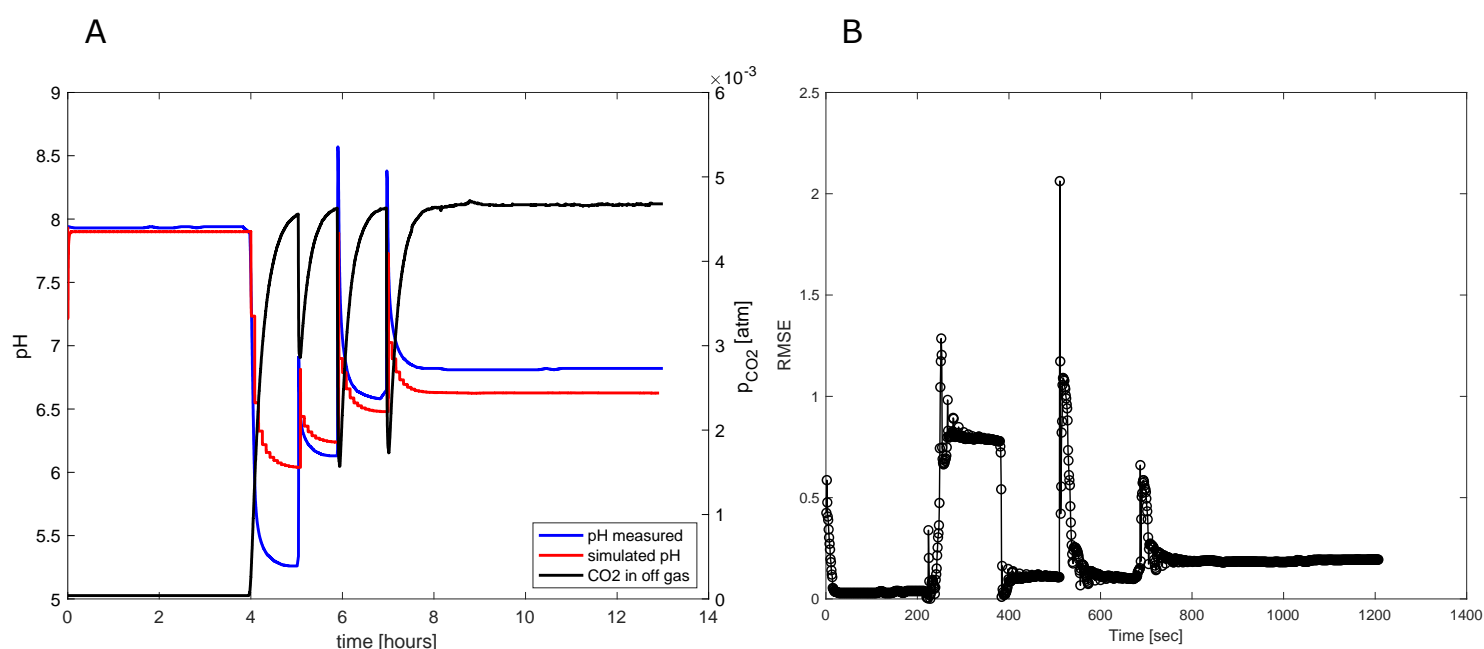

Figure 23. The CO_2 in the off-gas, the measured, and simulated pH in a solution (I = 0.5M, started at 1% v/v CO_2) with addition of NaOH (A). The Root Mean Square Error (RMSE) of the model estimation compared to the measured pH (B).
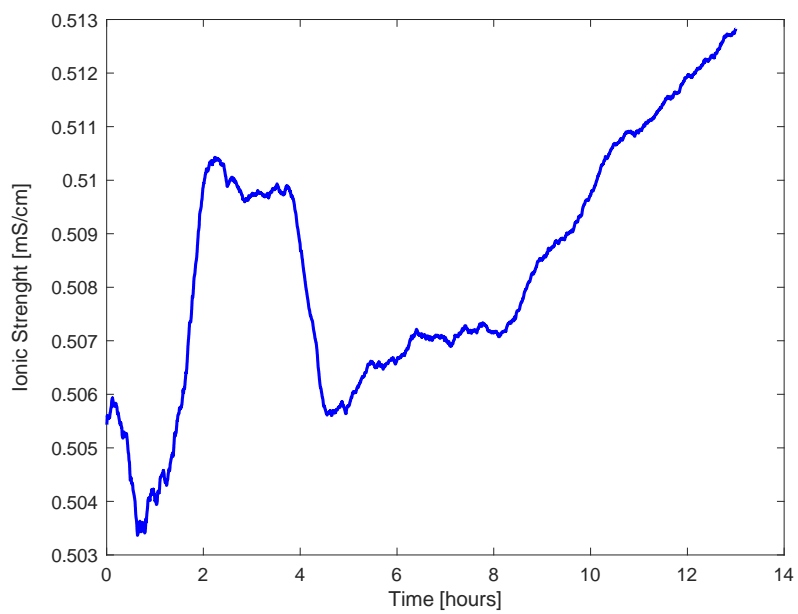
Figure 24. Ionic strength during the step wise addition of NaOH in a solution with an ionic strength of 0.5M.

5. Conclusions

The pH within a dynamic carbonate system can be predicted using a mathematical model implemented in MATLAB. The model considers the measured off-gas CO_2 concentrations and electrical conductivity measurements as input. It provides estimations for the concentrations of the species present in the carbonate system and calculates the pH over time.

The model's response follows the behavior of the measured pH values during the changing CO_2 concentrations in the different dilutions of ASW and undiluted ASW. However, when CO_2 concentrations approach 0% v/v during the desaturation process, a stepwise result of the modeled pH is obtained instead of a gradual change. This behavior can be attributed to the stepwise nature of the off-gas analyzer measurement data.

During the calibration experiments, the model exhibits different responses depending on the ionic strength of the ASW dilutions and undiluted ASW. Two different options for fitting the model during calibration are discussed. Setting the cation fit factor to fit during the initialization of the experiment (i.e. 0% v/v) lead to no direct correlation whereas fitting at 1% v/v CO_2 lead to a linear relationship. The relationship between the cation fit factor concentration and the ionic strength can be characterized by the equation $y = -0.0253x + 0.0213$, where y represents the cation concentration and x the ionic strength. The correlation coefficient (R^2) of 0.87 indicates a moderate linear relationship between the two variables. The two options, fitting the model during the initialization phase and fitting at a CO_2 concentration of 1% v/v, have both advantages and disadvantages.

For model validation, performed in a solution with an ionic strength of approximately 0.3M, the average RMSE was found to be 0.447. This indicates the level of deviation between the model's predication and the actual measured values during the validation experiment was marginal.

6. Recommendations

Further research is necessary to improve the accuracy of the model. In particular, the determination of the cation fit factor to calibrate the model needs further investigation. More datapoints are required to obtain an accurate result of the calibration. The current calibration is based on only five measurements, which may not be sufficient to predict an accurate cation fit factor. Especially, in the solutions with an ionic strength of 0.2M high deviations are found Furthermore, it is recommended to fit the model at a CO_2 concentration of approximately 0.5% v/v avoiding the uncertainty term of the off-gas CO_2 measurement when approaching a concentration of 0% v/v. Additionally, the accuracy of the calibration would be improved when fitting the model around neutral pH since the concentration of protons is lower around a pH of 7 than around a pH of 5. However, since the addition of 0.5% v/v CO_2 will ensure a decrease in the pH, fitting at neutral pH will not be feasible. Thus, fitting with the use of the cation fit factor would be ideally at a CO_2 concentration of 0.5% v/v in the off-gas and at a pH of approximately 6.

Also, it is recommended to investigate the formation of calcium carbonate in more saline solutions as it may contribute to the observed deviations between the measured and the predicted pH values. The slight precipitation of calcium carbonate could explain the lower pH measured at higher CO_2 concentrations and the higher pH measured at CO_2 concentrations approaching 0% v/v. By incorporating these dynamics into the model, more precise predictions of component concentrations and the pH of the solution can be achieved. Specifically, in solutions with higher ionic strengths where more calcium ions are present. This inclusion of the calcium carbonate kinetics should be incorporated in the model before more extensive calibration is performed.

Further recommendations mark to test the model in a pH range more closely related to algae cultivation. The current experiments primarily focussed on pH values ranging from 4 to 5.5. However, since microalgae cultivation often occurs at neutral pH, it is crucial to validate the model's performance in this pH range. Furthermore, simulating a more gradual increase or decrease in pH would provide insights into the model's behavior under such conditions. Conducting a dilution experiment with an incoming 0% v/v CO_2 concentration solution to gradually decrease the pH of the solution could facilitate a gradual decrease in pH.

Finally, to investigate the change of cation in the model such as in the experiment with NaOH addition, further experiments are required. The model should be adjusted to respond to varying cation concentrations instead of using a fixed concentration to account for the cation surplus present. By conducting these experiments and modifying the model accordingly, a more accurate representation of the changing cation dynamics can be achieved.

7. Acknowledgements

First of all, I want to thank Henrik Geltner for the supervision during the past 6 months. Especially, during the lab work and the practical work involved which is not my strongest aspect. Also, you helped me a lot when I got a bit lost personally. I appreciate that. Secondly, I would like to thank Marcel Janssen for sharing your thoughts and questions during our meetings. These helped me to take a step back out of the details of the model, review the overall use of it and get a better view of the bigger picture.

Furthermore, I want to thank all the students at the Bioprocess Engineering group for sharing their knowledge, help and the fun borrels we had. In particular, Inge Braak who joined me during every step and helped to get me through the tougher moments. Lastly, I want to thank my parents and friends for all the support.

8. Appendices

8.1 MATLAB model

8.1.1 Running model

```matlab
% clear output window, workspace and close graph windows
clc
clear
close all

%% Calculate the results
RunStart = 5930;              % Syntax of the starting point of your
experiment in the table Data_tot
RunEnd = 21560;               % Syntax of the ending point of your
experiment in the table Data_tot

% Extract the results from the function CalculateRun
runResult = CalculateRun("EC_0.5M.csv",
"06062023_Servomex_Data.txt","pH0_5.txt", 5930, 21560);

% pH and pCO2 measured
time = runResult.Time;
pH = runResult.Data_tot.pH;
CO2 = runResult.Data_tot.CO2_cor;

% pH simulation
t = runResult.tsim;
pH_sim = runResult.pHsim;

% RMSE
rmse = runResult.rmse;
num_rmse = runResult.num_rmse;

% Calculate the mean Root Mean Squared error of the run
mean_rmse = mean(rmse);

% Plot the change in ionic strength over time
figure(1)
plot(time(RunStart:RunEnd), runResult.Data_tot.I(RunStart:RunEnd), "-b",
"LineWidth", 2);
xlabel('Time [hours]');
ylabel('Ionic Strenght [M]')

% PLot the model predicted pH, measured pH and change in CO2 in the off-gas
figure(2)
colororder({'k','k'});
xlabel('Time [hours]');
yyaxis left
ylabel('pH')
    plot(time(RunStart:RunEnd),pH(RunStart:RunEnd),'-b','LineWidth',2);
hold on
    plot(t/(3600),pH_sim,'-r','LineWidth',2) ;
yyaxis right
ylabel('p_{CO2} [atm]');
    plot(time(RunStart:RunEnd),CO2(RunStart:RunEnd)/100,'-
k','LineWidth',2);
ylim([0 0.022]);
legend('pH measured','simulated pH','offgas xCO_{2} ');
```

```
% Plot RMSE values
figure(3)
plot(num_rmse, rmse, '-ko', 'LineWidth', 1);
xlabel('Time [sec]');
ylabel('RMSE');
title('0.5M RMSE');
```

8.1.2 Calculating Function

```
function [runResult] = CalculateRun(ECdataFile, CO2dataFile, pHdataFile,
RunStart, RunEnd)

    %% Load EC data
    EC_import = importEC(ECdataFile);

    % Combine date and time string to 1 string
    Datetime = strcat(char(EC_import.Date), " ", char(EC_import.Time));

    % Parsing datetime string to a date time object
    ECtime = datetime(Datetime, 'InputFormat', "dd/MMM/yyyy HH:mm:ss");

    % Get EC column filtered by NaNs
    EC1 = EC_import.Ch2_M1(~isnan(EC_import.Ch2_M1));

    % Smooth EC data
    EC = smoothdata(EC1);

    % Unit conversion: ms/cm to M
    I = 0.0127* EC- 0.0003;

    % Create a time vector with the same size as the EC vector
    TimeEC = ECtime(~isnan(EC_import.Ch2_M1));

    % Create new table including time steps
    ECv1 = table(TimeEC, I);

    % Rename columns in ECv1 table
    Table_EC1 = renamevars(ECv1, "TimeEC","Time");
    Table_EC = table2timetable(Table_EC1);



    %% Load CO2 offgas data

    % Import and clean file data
    CO2_import = importfile(CO2dataFile);

    % Combine date and time string to 1 string
    DateTime = strcat(char(CO2_import.Date), " ", char(CO2_import.Time));

    %Parsing datetime string to a date time object
    TimeCO2= datetime(DateTime, 'InputFormat', "dd.MMM.yyyy HH:mm:ss");

    % Get CO23 column filtered by NaNs
    CO2 = CO2_import.CO23(~isnan(CO2_import.CO23));

    % CO2 data correction based on the calibration curve of the dry base
line
    CO2_cor = CO2 / 0.9734;
```

```matlab
    % Create new tables including time steps
    Table_CO2 = table(TimeCO2, CO2_cor);
    Table_CO2 = renamevars(Table_CO2, "TimeCO2", "Time");
    Table_CO2 = table2timetable(Table_CO2);

    % Correct for noise in the CO2 data when approaching O% v/v
    indices = find(Table_CO2.CO2_cor < 0.004);
    Table_CO2.CO2_cor(indices) = 0.002;

    %% Load pH data from Infors 2 file
    % Load Water1_no_avgeraging txt file
    pH_import = importIrispH(pHdataFile);

    % Combine date and time string to 1 string
    f = strcat(char(pH_import.Date), " ", char(pH_import.Time));

    % Parsing datetime string to a date time object
    TimeVec = datetime(f, 'InputFormat', 'dd-MM-yy HH:mm:ss');

    % Get pH column filtered by NaNs
    pH = pH_import.pH(~isnan(pH_import.pH));

    % Create a time vector with the same size as the pH vector
    TV = TimeVec(~isnan(pH_import.pH));

    % Create new table including time strings
    Table_pH = table(TV,pH);

    % Rename time column in I0_pH table
    Table_pH = renamevars(Table_pH, ["TV"], ["Time"]);
    Table_pH = table2timetable(Table_pH);

    % Synchronize pH, EC and CO2 tables
    Data_tot = synchronize(Table_pH, Table_CO2, 'union', 'linear');
    Data_tot = synchronize(Data_tot, Table_EC, 'union', 'linear');

    % Calculation of RunTime in seconds and hours subsequently
    T_s =
day(Data_tot.Time)*24*3600+hour(Data_tot.Time)*3600+minute(Data_tot.Time)*6
0+second(Data_tot.Time)-
(day(Data_tot.Time(RunStart))*24*3600+hour(Data_tot.Time(RunStart))*3600+mi
nute(Data_tot.Time(RunStart))*60+second(Data_tot.Time(RunStart)));
    T_h = T_s/3600;

    %% Simulate pH based on CO2 partial pressure in the offgas and EC
measurements

    % Initialize start values
    pHstart = Data_tot.pH(RunStart);       % Start pH
    I_0 = Data_tot.I(RunStart);            % Start ionic strenght[M]
    gamma_1=0.7;                           % Estimation based on
literature
    gamma_2=0.038;                         % Estimation based on
literature

    % Pre-allocate concentration vector assuming the bioreactor is
completely stripped from CO2
```

```matlab
    concentration=[0 0 0 (10^(-pHstart))/gamma_1 (10^-(14-pHstart))/gamma_1
0 I_0 gamma_1 gamma_2 0];

    % Set fit factor (cation concentration) at t0
    concentration(6) = 1.1E-5;

    % Initialize the bicarbonate concentration equal to [cation]
    concentration(2) = concentration(6);

    % Initialize the counter of the loop to zero seconds
    t0 = 0;
    time=0;

    % Set upper value for timeInterval in which the ODE solver ode15s will
run each simulation
    tt = 5 * 60;

    % Set the length of the run in seconds
    tl = T_s(RunEnd) - T_s(RunStart);

    while t0+tt < tl

        % find the current T_s value so we can lookup data in Data_tot
        s = find(T_s < (t0), 1, 'last') + 1;

        % lookup current values in Data_tot
        I = Data_tot.I(s);
        c_CO2 = Data_tot.CO2_cor(s);

         % Update concentration vector based on t and pHstart
         c0=[concentration(end,1)
             concentration(end,2)
             concentration(end,3)
             (10^(-pHstart))/gamma_1
             (10^-(14-pHstart))/gamma_1
             concentration(end,6)
             I
             concentration(end,8)
             concentration(end,9)
             c_CO2/100];

        % Define ODE system
        odefun = @(t, cl) CO2sys(t, cl);
        % Resolution settings for ODEsolver
        opts = odeset('RelTol',1e-8,'AbsTol',1e-10);
        % Apply ODE for the model
        [t, cl] = ode15s(odefun,[t0 t0+tt],c0,opts);

        % Storing time steps
        time = [time;t];

        % Storing the newly calculated concentrations
        concentration = [concentration;cl];

        % new pH for initializing model
        pHstart = -log10(cl(end,4)*gamma_1);

        % Next initial time for simulation at the endptime of last interval
```

```matlab
    t0 = t0 + tt;
end

cl=concentration; % Final writing to one vector
t=time;           % Rename

% pH calculation
ph = -log10(cl(:,4).*cl(:,8));

%% RMSE

% Time in seconds
time_m = T_s(RunStart:RunEnd);
time_s = t;

% Calculate the number of seconds
num_sec = floor(max(time_s));

% Initialize arrays to store RMSE values for each second
rmse_values = zeros(num_sec, 1);

% Calculate RMSE for each second
    for sec = 1:num_sec

        % Find the indices corresponding to the current second
        indices_m = find(time_m >= sec-1 & time_m < sec);
        indices_s = find(time_s >= sec-1 & time_s < sec);

        % Extract pH data for the current second
        pH_measured = Data_tot.pH(RunStart:RunEnd);
        pH_m = pH_measured(indices_m);
        pH_s = mean(ph(indices_s));

        % Calculate the squared differences for the current second
        squared_diffs = (pH_m - pH_s).^2;

        % Calculate the mean squared difference for the current second
        mean_squared_diff = mean(squared_diffs);

        % Calculate the RMSE for the current second
        rmse_sec = sqrt(mean_squared_diff);

        % Store the RMSE value for the current second
        rmse_values(sec) = rmse_sec;
    end

    % Filter NaN values out
    rmse = rmse_values(~isnan(rmse_values));
    num_rmse = 1:length(rmse);

%% Return the calculate run result
runResult.Data_tot = Data_tot;
runResult.Time = T_h;
runResult.pHsim = ph;
runResult.tsim = t;
runResult.concentration = cl;
runResult.rmse = rmse;
runResult.num_rmse = num_rmse;
```

```
end
```

8.1.3 Function describing the Carbonate System

8.1.3.1 Carbonate System when ionic strength is lower than 0.5M

```matlab
function [dc] = CO2sys(~,dc)
% This function describes the ODE to be solved resulting in a matrix
% containing concentrations of the species in the carbonate system and its
% equilibria constants, activity coefficient and ionic strenght

% Load file with constants
Constants=Constants_Nanno();

    % Extract constants
    kLa=Constants.kla_CO2;
    HenryK=Constants.Hk;
    pK1_0=Constants.pK1_0;
    pK2_0=Constants.pK2_0;
    Kw=Constants.Kw;
    T=Constants.T;
    P = Constants.P;


    gamma_CO2=1.01;

    % Calculate ionic strenght and activity coefficients
    %I = 0.5*(dc(2) + 4*dc(3) + dc(4) + dc(5) + dc(6))+ I_0;
    I = dc(7);
    gamma_z1 = 10^(-((0.5 * (I^(1/2) / (1 + I^(1/2)))) - (0.3 * I)));
    gamma_z2 = 10^(-((0.5 * 4 * (I^(1/2) / (1 + I^(1/2)))) - (0.3 * I)));

    A1 = 93.9053*I^(0.5) + 1.6549*I - 0.130*I^2;
    A2 = 147.2748*I^(0.5) + 6.0876*I - 0.8691*I^2;
    B1 = -3706.9*I^(0.5) - 303.7*I;
    B2 = -5400.9*I^(0.5) - 968.4*I;
    C1 = -14.4858*I^(0.5);
    C2 = -23.2804*I^(0.5);

    pK1 = pK1_0 + A1 +B1/T + C1*log(T);
    pK2 = pK2_0 + A2 + B2/T + C2*log(T);
    K1 = ((gamma_z1*gamma_z1)/(gamma_CO2))*10^-pK1;
    K2 = ((gamma_z1*gamma_z2)/gamma_z1)*10^-pK2;

    % Calculate new concentration values
     c_CO2 = kLa*(dc(10)*P*HenryK-dc(1))-
(((gamma_CO2/(gamma_z1*gamma_z1))*K1*dc(1)/dc(4))-dc(2));
     c_HCO3 = ((gamma_CO2/(gamma_z1*gamma_z1))*K1*dc(1)/dc(4))-dc(2)-
(((gamma_z1/(gamma_z2*gamma_z1))*K2*dc(2)/dc(4))-dc(3));
     c_CO3 = (gamma_z1/(gamma_z2*gamma_z1)*K2*dc(2)/dc(4))-dc(3);
     c_H =  dc(2)+2*dc(3)+dc(5)-dc(4)-dc(6);
     c_OH = 1/(gamma_z1*gamma_z1)*Kw/dc(4) - dc(5);

    dc=[  c_CO2;
          c_HCO3;
          c_CO3;
          c_H;
          c_OH;
          0;
          0;
          gamma_z1 - dc(8);
          gamma_z2- dc(9);
          0;];
end
```

8.1.3.2 Carbonate System when ionic strength exceeds 0.5M

```matlab
function [dc] = CO2sys(~,dc)
% This function describes the ODE to be solved resulting in a matrix
% containing concentrations of the species in the carbonate system and its
% equilibria constants, activity coefficient and ionic strenght

% Load file with constants
Constants = Constants();

    % Extract constants
    kLa = Constants.kla_CO2;
    HenryK = Constants.Hk;
    pK1_0 = Constants.pK1_0;
    pK2_0 = Constants.pK2_0;
    Kw = Constants.Kw;
    T = Constants.T;
    P = Constants.P;

    % Calculate ionic strenght and activity coefficients
    I = dc(7);
    gamma_OH = 10^(-((0.5 * (I^(1/2) / (1 + I^(1/2)))) - (0.3 * I)));
    gamma_H = 0.0728*I +0.6636;
    gamma_HCO3 = -0.2756*I + 0.6837;
    gamma_CO3 = -0.0689*I + 0.0783;
    gamma_CO2 = -0.0252*I + 0.9974;
    a_H2O = -0.0326*I + 1.0035;

    A1 = 93.9053*I^(0.5) + 1.6549*I - 0.130*I^2;
    A2 = 147.2748*I^(0.5) + 6.0876*I - 0.8691*I^2;
    B1 = -3706.9*I^(0.5) - 303.7*I;
    B2 = -5400.9*I^(0.5) - 968.4*I;
    C1 = -14.4858*I^(0.5);
    C2 = -23.2804*I^(0.5);

    pK1 = pK1_0 + A1 +B1/T + C1*log(T);
    pK2 = pK2_0 + A2 + B2/T + C2*log(T);
    K1 = ((gamma_H*gamma_HCO3)/(a_H2O*gamma_CO2))*10^-pK1;
    K2 = ((gamma_H*gamma_CO3)/gamma_HCO3)*10^-pK2;

    % Calculate new concentration values
    c_CO2 = kLa*(dc(10)*P*HenryK-dc(1))-
((((gamma_CO2*a_H2O)/(gamma_HCO3*gamma_H))*K1*dc(1)/dc(4))-dc(2));
    c_HCO3 = (((gamma_CO2*a_H2O)/(gamma_HCO3*gamma_H))*K1*dc(1)/dc(4))-
dc(2)-(((gamma_HCO3/(gamma_CO3*gamma_H))*K2*dc(2)/dc(4))-dc(3));
    c_CO3 = (gamma_HCO3/(gamma_CO3*gamma_H)*K2*dc(2)/dc(4))-dc(3);
    c_H =  dc(2)+2*dc(3)+dc(5)-dc(4)-dc(6);
    c_OH = 1/(gamma_H*gamma_OH)*Kw/dc(4) - dc(5);

    % ODE input
    dc=[  c_CO2;
          c_HCO3;
          c_CO3;
          c_H;
          c_OH;
          0;
          0;
          gamma_H - dc(8);
          0;
```

```matlab
                0;];
    end
```

8.1.4 Constants

```matlab
function Constants
% This function gives out a table Constants, which contains the
% constant parameters set for pH simulation in ASW at moderate temperature

Constants.T=298.15; % Kelvin

WaterColumn = 16; % overpressure measured [cm]
        R_h = 41 + WaterColumn;   %  height of the reactor [cm]
        P_atm = 1.01325; % bar
        P_cm = 0.001;    % bar, assuming pressure increases 0.1 bar per
meter
Constants.P = (P_atm+(R_h/2)*P_cm)/P_atm;

        T=Constants.T;
Constants.pK1_0 = -126.34048 + 6320.813/T +19.568224*log(T);
Constants.pK2_0 = -90.18333 + 5143.692/T + 14.613358*log(T);

        kla_O2=0.323;
Constants.kla_O2=kla_O2;         %6 kla in s^(-1) O2
Constants.kla_CO2=0.89*kla_O2*10;        %7 kla in s^(-1) CO2;
Constants.Kw=10^(-14);

H_Tref =  0.033;     % Henry constant 298.15K [mol/L/bar]
ks = 0.089;          % Sechenov constant 298.15K for CO2 in NaCl solution
Constants.Hk =  H_Tref/(10^(-ks*I));
end
```

8.1.5 Import EC Data Function

```matlab
function EC = importEC(filename)
%% Set up the Import Options and import the data
opts = delimitedTextImportOptions("NumVariables", 10);

% Specify range and delimiter
dataLines = [2, Inf];
opts.DataLines = dataLines;
opts.Delimiter = ",";

% Specify column names and types
opts.VariableNames = ["Date", "Time", "Ch2_M1", "Ch2_M1Unit", "Ch2_M2",
"Ch2_M2Unit", "Ch2_M3", "Ch2_M3Unit", "Ch2_M4", "Ch2_M4Unit"];
opts.SelectedVariableNames = ["Date", "Time", "Ch2_M1"];
opts.VariableTypes = ["char", "char", "double", "char", "char", "char",
"char", "char", "char", "char"];

% Specify file level properties
opts.ExtraColumnsRule = "ignore";
opts.EmptyLineRule = "read";

% Specify variable properties
opts = setvaropts(opts, ["Date", "Time", "Ch2_M1", "Ch2_M1Unit", "Ch2_M2",
"Ch2_M2Unit", "Ch2_M3", "Ch2_M3Unit", "Ch2_M4", "Ch2_M4Unit"],
"EmptyFieldRule", "auto");
```

```matlab
% Import the data
EC = readtable(filename, opts);
end
```

8.1.6 Import pH Data Function

```matlab
function pHfile = importIrispH(filename, dataLines)
% If dataLines is not specified, define defaults
if nargin < 2
    dataLines = [7, Inf];
end

%% Set up the Import Options and import the data
opts = delimitedTextImportOptions("NumVariables", 21);

% Specify range and delimiter
opts.DataLines = dataLines;
opts.Delimiter = ",";

% Specify column names and types
opts.VariableNames = ["Date", "Time", "Temp", "pH", "Var5", "Var6", "Var7",
"Var8", "Var9", "Var10", "Var11", "Var12", "Var13", "Var14", "Loop",
"Var16", "Var17", "Var18", "Var19", "Var20", "Var21"];
opts.SelectedVariableNames = ["Date", "Time", "Temp", "pH", "Loop"];
opts.VariableTypes = ["datetime", "datetime", "double", "double", "char",
"char", "char", "char", "char", "char", "char", "char", "char",
"double", "char", "char", "char", "char", "char", "char"];

% Specify file level properties
opts.ExtraColumnsRule = "ignore";
opts.EmptyLineRule = "read";

% Specify variable properties
opts = setvaropts(opts, ["Var5", "Var6", "Var7", "Var8", "Var9", "Var10",
"Var11", "Var12", "Var13", "Var14", "Var16", "Var17", "Var18", "Var19",
"Var20", "Var21"], "WhitespaceRule", "preserve");
opts = setvaropts(opts, ["Var5", "Var6", "Var7", "Var8", "Var9", "Var10",
"Var11", "Var12", "Var13", "Var14", "Var16", "Var17", "Var18", "Var19",
"Var20", "Var21"], "EmptyFieldRule", "auto");
opts = setvaropts(opts, "Date", "InputFormat", "dd-MM-yy");
opts = setvaropts(opts, "Time", "InputFormat", "HH:mm:ss");

% Import the data
pHfile = readtable(filename, opts);


end
```

8.1.7 Import Off-gas Analysis Data Function

```matlab
function CO2 = importfile(filename)
%% Set up the Import Options and import the data
opts = delimitedTextImportOptions("NumVariables", 10);

% Specify range and delimiter
dataLines = [2, Inf];
opts.DataLines = dataLines;
opts.Delimiter = ";";

% Specify column names and types
opts.VariableNames = ["Date", "Time", "Oxygen1", "Oxygen1", "CO22", "CO22",
"Oxygen3", "CO23", "Oxygen4", "CO24"];
opts.SelectedVariableNames = ["Date", "Time", "CO23"];
opts.VariableTypes = ["char", "char", "char", "char", "char", "char",
"char", "double", "char", "char"];
```

```matlab
% Specify file level properties
opts.ExtraColumnsRule = "ignore";
opts.EmptyLineRule = "read";

% Specify variable properties
% opts = setvaropts(opts, ["Date", "Time", "Oxygen1", "Oxygen1", "CO22",
"CO22", "Oxygen3", "CO23", "Oxygen4", "CO24"], "WhitespaceRule",
"preserve");
opts = setvaropts(opts, ["Date", "Time", "Oxygen1", "Oxygen1", "CO22",
"CO22", "Oxygen3", "CO23", "Oxygen4", "CO24"], "EmptyFieldRule", "auto");

% Import the data
CO2 = readtable(filename, opts);

end
```
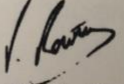
8.2 Sensor Probe Quality Certificates

8.2.1 pH Sensor InPro3030

pH Sensor InPro3030/120
Part No. 52001310

Serial No. 3084693

	Specification / Spezifikation / Spécification
Value at 25°C / Messgrösse bei 25°C / Valeur à 25°C	
Slope pH 4...7, % of theoretical value / Steilheit pH 4...7, % vom theoretischen Wert / Pente à pH 4...7, % de la valeur théorique	> 98 %
Zero point / Nullpunkt / Point zéro	pH 7.00 +/- 0.25
Membrane resistance / Membranwiderstand / Résistance de membrane	< 500 MOhm
Response time (98% between pH 4...7) / Ansprechzeit (98% zwischen pH 4...7) / Temps de réponse (98% entre pH 4...7)	< 20 sec

Quality Control passed.
Qualitätsprüfung bestanden.
Satisfait au contrôle qualité.

Quality Manager
Peter Rowing   2023-02-23

QC — Quality Certified — METTLER TOLEDO — Quality Applied

8.2.2 EC Sensor Inpro 7100i

Quality Certificate
Qualitäts-Zertifikat
Certificat de Qualité

InPro7100i/12/120/C22

Part No./Artikel-Nr./   52003792
Numeró de commande
Serial No./Serien-Nr./   2244015
Numeró de serie
Cell constant/Zelkonstante/   Nominal 0.300 cm^{-1}
Constante de cellule
Cell adder/Additionsfaktor/Facteur Additif   -0.022885
Date/Datum/Date   14-Nov-2022
Actual cell constant/   0.269482 cm^{-1}
Aktuelle Zellkonstante/
Actuelle consfante de cellule

Temperature Sensor: NTC 30k
Temperatursensor/senseur de temprature
Measuring range: 0.02-500 mS/cm
Messbereich/etendue de mesure
Sensor technology: 4-pol contacting
Process connection: PG13.5

Calibration Data/Kalibrationsdaten/
Donneeś de calibration:
Temp.   20.27 ^{0} C
Cond1   1.179   mS/cm (1.179   mS/cm)
Cond2   83.351   mS/cm (83.339   mS/cm)

Quality Control passed.
Qualitätsprüfung bestanden.
Satisfait au contrôle qualité.

QC — METTLER TOLEDO — Quality Certified

METTLER TOLEDO

8.2.3 Dissolved CO$_2$ Sensor RS485 120

Declaration of Quality

CO$_2$NTROL RS485 120

Product Identification

Ref	10087810-11
SN	1581
Lot	111319345
Heat Numbers	285215 / 641079
Firmware	COOUM003

Factory Test Conditions

Tests were performed according to	111002142
Temperature	29.0 °C
Ambient pressure	944.0 mbar

Factory Test Results

	Test Specification	Result
Certified Gas Standard 20.0% Vol CO$_2$	20.0 ± 1.0 % Vol CO$_2$	20.26 % Vol CO$_2$
Quality Indicator	100 %	passed
Quality Test successfully passed	**2022-07-21**	

HAMILTON PASSED QUALITY CONTROL

This declaration is generated automatically and valid without signature.

REF

HAMILTON
Web: www.hamiltoncompany.com
USA: 800-648-5950

Hamilton Americas & Pacific Rim
4970 Energy Way
Reno, Nevada 89502 USA
Tel: +1-775-858-3000
Fax: +1-775-856-7259
sales@hamiltoncompany.com

Hamilton Europe,
Via Crusch 8
CH-7402 Bonaduz, Switz
Tel: +41-58-610-10-10
Fax: +41-58-610-00-10
contact.pa.ch@hamilton.ch

References

Barrut, B., Blancheton, J.-P., Champagne, J.-Y., & Grasmick, A. (2012). Mass transfer efficiency of a vacuum airlift—Application to water recycling in aquaculture systems. *Aquacultural Engineering*, *46*, 18–26. https://doi.org/10.1016/j.aquaeng.2011.10.004

Berenguel, M., Rodríguez, F., Acién, F. G., & García, J. L. (2004). Model predictive control of pH in tubular photobioreactors. *Journal of Process Control*, *14*(4), 377–387. https://doi.org/10.1016/j.jprocont.2003.07.001

Boogerd, F. C., Bos, P., Kuenen, J. G., Heijnen, J. J., & van der Lans, R. G. J. M. (1990). Oxygen and carbon dioxide mass transfer and the aerobic, autotrophic cultivation of moderate and extreme thermophiles: A case study related to the microbial desulfurization of coal. *Biotechnology and Bioengineering*, *35*(11), 1111–1119. https://doi.org/10.1002/bit.260351106

Buck, R. P., Rondinini, S., Covington, A. K., Baucke, F. G. K., Brett, C. M. A., Camoes, M. F., Milton, M. J. T., Mussini, T., Naumann, R., Pratt, K. W., Spitzer, P., & Wilson, G. S. (2002). Measurement of pH. Definition, standards, and procedures (IUPAC Recommendations 2002). *Pure and Applied Chemistry*, *74*(11), 2169–2200. https://doi.org/10.1351/pac200274112169

Caizán-Juanarena, L., ter Heijne, A., Weijma, J., Yntema, D., Suárez-Zuluaga, D. A., & Buisman, C. J. N. (2020). Screening for electrical conductivity in anaerobic granular sludge from full-scale wastewater treatment reactors. *Biochemical Engineering Journal*, *159*, 107575. https://doi.org/10.1016/j.bej.2020.107575

Cuaresma, M., Janssen, M., Vílchez, C., & Wijffels, R. H. (2011). Horizontal or vertical photobioreactors? How to improve microalgae photosynthetic efficiency. *Bioresource Technology*, *102*(8), 5129–5137. https://doi.org/10.1016/j.biortech.2011.01.078

Culberson, C. H., & Pytkowicz, R. M. (1973). Ionization of water in seawater. *Marine Chemistry*, *1*(4), 309–316. https://doi.org/10.1016/0304-4203(73)90020-0

Dochain, D. (2013). *Automatic Control of Bioprocesses*. John Wiley & Sons.

Elhajj, J., Al-Hindi, M., & Azizi, F. (2014). A Review of the Absorption and Desorption Processes of Carbon Dioxide in Water Systems. *Industrial & Engineering Chemistry Research*, *53*(1), 2–22. https://doi.org/10.1021/ie403245p

Eriksen, N. T., Riisgård, F. K., Gunther, W. S., & Lønsmann Iversen, J. J. (2007). On-line estimation of O2 production, CO2 uptake, and growth kinetics of microalgal cultures in a gas-tight photobioreactor. *Journal of Applied Phycology*, *19*(2), 161–174. https://doi.org/10.1007/s10811-006-9122-y

Fernández, V. M. (2011). Water Activity. In M. Gargaud, R. Amils, J. C. Quintanilla, H. J. (Jim) Cleaves, W. M. Irvine, D. L. Pinti, & M. Viso (Eds.), *Encyclopedia of Astrobiology* (pp. 1763–1764). Springer. https://doi.org/10.1007/978-3-642-11274-4_1678

Fortuna, L. (Luigi). (2007). *Soft sensors for monitoring and control of industrial processes* (1–1 online resource (xviii, 270 pages) : illustrations). Springer. http://site.ebrary.com/id/10181018

Galaction, A.-I., Cascaval, D., Oniscu, C., & Turnea, M. (2004). Prediction of oxygen mass transfer coefficients in stirred bioreactors for bacteria, yeasts and fungus broths. *Biochemical Engineering Journal*, *20*(1), 85–94. https://doi.org/10.1016/j.bej.2004.02.005

Garfinkel, D., Marbach, C. B., & Shapiro, N. Z. (1977). Stiff Differential Equations. *Annual Review of Biophysics and Bioengineering*, *6*(1), 525–542. https://doi.org/10.1146/annurev.bb.06.060177.002521

González-Camejo, J., Robles, A., Seco, A., Ferrer, J., & Ruano, M. V. (2020). On-line monitoring of photosynthetic activity based on pH data to assess microalgae cultivation. *Journal of Environmental Management*, *276*, 111343. https://doi.org/10.1016/j.jenvman.2020.111343

Griffin, R. A., & Jurinak, J. J. (1973). Estimation of activity coefficients from the electrical conductivity of natural aquatic systems and soil extracts. *Soil Science*. https://scholar.google.com/scholar_lookup?title=Estimation+of+activity+coefficients+from+the+electrical+conductivity+of+natural+aquatic+systems+and+soil+extracts&author=Griffin%2C+R.A.&publication_year=1973

Guldhe, A., Kumari, S., Ramanna, L., Ramsundar, P., Singh, P., Rawat, I., & Bux, F. (2017). Prospects, recent advancements and challenges of different wastewater streams for microalgal cultivation. *Journal of Environmental Management*, *203*, 299–315. https://doi.org/10.1016/j.jenvman.2017.08.012

Harned, H. S., & Davis, R. (1943). The Ionization Constant of Carbonic Acid in Water and the Solubility of Carbon Dioxide in Water and Aqueous Salt Solutions from 0 to 50°. *Journal of the American Chemical Society*, *65*(10), 2030–2037. https://doi.org/10.1021/ja01250a059

Harned, H. S., & Scholes, S. R. (1941). The Ionization Constant of HCO $_3$—From 0 to 50°. *Journal of the American Chemical Society*, *63*(6), 1706–1709. https://doi.org/10.1021/ja01851a058

Haynes, W. M. (2010). *CRC Handbook of Chemistry and Physics.* (91st ed.). CRC Press Inc.

Hodson, T. O. (2022). Root-mean-square error (RMSE) or mean absolute error (MAE): When to use them or not. *Geoscientific Model Development*, *15*(14), 5481–5487. https://doi.org/10.5194/gmd-15-5481-2022

Ifrim, G. A., Titica, M., Cogne, G., Boillereaux, L., Legrand, J., & Caraman, S. (2014). Dynamic pH model for autotrophic growth of microalgae in photobioreactor: A tool for monitoring and control purposes. *AIChE Journal*, *60*(2), 585–599. https://doi.org/10.1002/aic.14290

IUPAC-NIST Solubilities Database. (n.d.). Retrieved June 1, 2023, from https://srdata.nist.gov/solubility/sol_detail.aspx?sysID=62_73

Jiang, Y., Yin, S., Dong, J., & Kaynak, O. (2021). A Review on Soft Sensors for Monitoring, Control, and Optimization of Industrial Processes. *IEEE Sensors Journal*, *21*(11), 12868–12881. https://doi.org/10.1109/JSEN.2020.3033153

Kadlec, P., Gabrys, B., & Strandt, S. (2009). Data-driven Soft Sensors in the process industry. *Computers & Chemical Engineering*, *33*(4), 795–814. https://doi.org/10.1016/j.compchemeng.2008.12.012

Li, C., Lesnik, K. L., & Liu, H. (2017). Stay connected: Electrical conductivity of microbial aggregates. *Biotechnology Advances*, *35*(6), 669–680. https://doi.org/10.1016/j.biotechadv.2017.07.010

Millero, F. J., Graham, T. B., Huang, F., Bustos-Serrano, H., & Pierrot, D. (2006). Dissociation constants of carbonic acid in seawater as a function of salinity and temperature. *Marine Chemistry*, *100*(1), 80–94. https://doi.org/10.1016/j.marchem.2005.12.001

Moran, D. (2010). Carbon dioxide degassing in fresh and saline water. II: Degassing performance of an air-lift. *Aquacultural Engineering*, *43*(3), 120–127. https://doi.org/10.1016/j.aquaeng.2010.09.001

Naumann, R., Alexander-Weber, Ch., Eberhardt, R., Giera, J., & Spitzer, P. (2002). Traceability of pH measurements by glass electrode cells: Performance characteristic of pH electrodes by multi-point calibration. *Analytical and Bioanalytical Chemistry*, *374*(5), 778–786. https://doi.org/10.1007/s00216-002-1506-5

Ndiaye, M., Gadoin, E., & Gentric, C. (2018). CO2 gas–liquid mass transfer and kLa estimation: Numerical investigation in the context of airlift photobioreactor scale-up. *Chemical Engineering Research and Design*, *133*, 90–102. https://doi.org/10.1016/j.cherd.2018.03.001

Odendaal, H. M., & Jones, T. (2014). Actuator fault detection and isolation: An optimised parity space approach. *Control Engineering Practice*, *26*, 222–232. https://doi.org/10.1016/j.conengprac.2014.01.013

Olsen, J. E., Dunnebier, D., Davies, E., Skjetne, P., & Morud, J. (2017). Mass transfer between bubbles and seawater. *Chemical Engineering Science*, *161*, 308–315. https://doi.org/10.1016/j.ces.2016.12.047

Pankow, J. F. (2019). *Aquatic Chemistry Concepts, Second Edition*. CRC Press.

Plummer, L. N., & Sundquist, E. T. (1982). Total individual ion activity coefficients of calcium and carbonate in seawater at 25°C and 35%. Salinity, and implications to the agreement between apparent and thermodynamic constants of calcite and aragonite. *Geochimica et Cosmochimica Acta*, *46*(2), 247–258. https://doi.org/10.1016/0016-7037(82)90252-6

Pytkowicz, R. M. (1975). Activity coefficients of bicarbonates and carbonates in seawater1. *Limnology and Oceanography*, *20*(6), 971–975. https://doi.org/10.4319/lo.1975.20.6.0971

Ritsema, C. J. (1993). Estimation of activity coefficients of individual ions in solutions with ionic strengths up to 0.3 mol dm−3. *Journal of Soil Science*, *44*(2), 307–315. https://doi.org/10.1111/j.1365-2389.1993.tb00454.x

R.M. Boom, A.E.M. Janssen, M. Vermuë, M.A. Schutyser, G. Olivieri. (2021). *Transfer Processes Theory*. Agrotechnology and Food Sciences Group Food and Bioprocess Engineering.

Sander, R. (2015). Compilation of Henry's law constants (version 4.0) for water as solvent. *Atmospheric Chemistry and Physics*, *15*(8), 4399–4981. https://doi.org/10.5194/acp-15-4399-2015

Sander, R., Acree, W. E., Visscher, A. D., Schwartz, S. E., & Wallington, T. J. (2022). Henry's law constants (IUPAC Recommendations 2021). *Pure and Applied Chemistry*, *94*(1), 71–85. https://doi.org/10.1515/pac-2020-0302

Shampine, L. F., & Reichelt, M. W. (1997). The MATLAB ODE Suite. *SIAM Journal on Scientific Computing*, *18*(1), 1–22. https://doi.org/10.1137/S1064827594276424

Stumm, W. (1996). *Aquatic chemistry: Chemical equilibria and rates in natural waters* (3rd ed.). Wiley.

Suh, I. S., & Lee, C.-G. (2003). Photobioreactor engineering: Design and performance. *Biotechnology and Bioprocess Engineering*, *8*(6), 313–321. https://doi.org/10.1007/BF02949274

Tham, M. T., Montague, G. A., Julian Morris, A., & Lant, P. A. (1991). Soft-sensors for process estimation and inferential control. *Journal of Process Control*, *1*(1), 3–14. https://doi.org/10.1016/0959-1524(91)87002-F

Thermo Fisher Scientific. (2012). *Measuring pH of Pure Water and Other Low Conductivity Waters*.

Tokumura, M., Baba, M., Znad, H. T., Kawase, Y., Yongsiri, C., & Takeda, K. (2006). Neutralization of the Acidified Seawater Effluent from the Flue Gas Desulfurization Process: Experimental Investigation, Dynamic Modeling, and Simulation. *Industrial & Engineering Chemistry Research*, *45*(18), 6339–6348. https://doi.org/10.1021/ie0603619

Ulfsbo, A., Abbas, Z., & Turner, D. R. (2015). Activity coefficients of a simplified seawater electrolyte at varying salinity (5–40) and temperature (0 and 25°C) using Monte Carlo simulations. *Marine Chemistry*, *171*, 78–86. https://doi.org/10.1016/j.marchem.2015.02.006

Zeebe, R. E., & Wolf-Gladrow, D. (2001). *CO2 in Seawater: Equilibrium, Kinetics, Isotopes*. Gulf Professional Publishing.